

Circadian clock disruption promotes the degeneration of dopaminergic neurons in male *Drosophila*

Received: 7 October 2022

Michaëla Majcin Dorcikova¹, Lou C. Duret¹, Emma Pottié¹ & Emi Nagoshi¹✉

Accepted: 8 September 2023

Published online: 22 September 2023

 Check for updates

Sleep and circadian rhythm disruptions are frequent comorbidities of Parkinson's disease (PD), a disorder characterized by the progressive loss of dopaminergic (DA) neurons in the substantia nigra. However, the causal role of circadian clocks in the degenerative process remains uncertain. We demonstrated here that circadian clocks regulate the rhythmicity and magnitude of the vulnerability of DA neurons to oxidative stress in male *Drosophila*. Circadian pacemaker neurons are presynaptic to a subset of DA neurons and rhythmically modulate their susceptibility to degeneration. The arrhythmic *period (per)* gene null mutation exacerbates the age-dependent loss of DA neurons and, in combination with brief oxidative stress, causes premature animal death. These findings suggest that circadian clock disruption promotes dopaminergic neurodegeneration.

Disturbances in the sleep-wake rhythm are well-described symptoms in neurodegenerative disorders such as Parkinson's disease (PD)¹. PD is a complex disorder characterized by the progressive loss of dopaminergic (DA) neurons in the substantia nigra pars compacta, leading to motor symptoms². Sleep and circadian disruption can be observed years before the onset of motor symptoms³, raising the possibility that circadian rhythm disruption precedes and contributes to PD development. Studies using animal models of PD showed that circadian disruption could exacerbate neurodegeneration and motor symptoms⁴. However, it remains elusive whether circadian disturbances causally drive neurodegeneration or are caused by neurodegeneration, partly because PD pathology includes dysfunction of the brain regions regulating sleep, resulting in disrupted sleep-wake cycles⁵. Dissecting mechanistic links between circadian clock disruption and neurodegeneration—two intertwined and potentially synergistic processes—is critical for developing reliable diagnostic tools and treatment strategies for PD.

Drosophila melanogaster is a genetically tractable model system for studying neurodegenerative diseases⁶. Taking advantage of the conservation of PD-related molecular genetic pathways, numerous genetic and toxin-induced models of PD that display varying degrees of neurodegeneration and motor and non-motor symptoms have been generated^{7,8}. The adult fly midbrain contains approximately eight

clusters of DA neurons projecting to various brain regions⁹. Functional impairments or loss of DA neurons in the protocerebral anterior medial (PAM) and protocerebral anterior lateral 1 (PPL1) clusters have been consistently observed in PD models, in addition to the losses in other clusters^{10–15}. The PAM cluster comprises ~130 neurons per hemisphere, accounting for approximately 80% of fly brain DA neurons. PAM neurons are highly heterogeneous in their projection patterns and functions and play critical roles in behavioral processes such as olfactory associative learning, foraging, sleep, and locomotion^{16–20}. We and others showed that the loss of a subclass of PAM neurons leads to defective startle-induced climbing behavior in several PD models^{13,14,21}, suggesting a partial analogy between the PAM cluster and the substantia nigra pars compacta.

Circadian clocks, built upon the conserved design principle of negative feedback loops, drive rhythms in numerous behavioral and physiological processes in species across phylogenetic trees. The core feedback loop of the *Drosophila* circadian clock consists of CLOCK/CYCLE (CLK/CYC) heterodimers that activate transcription of the *period (per)* and *timeless (tim)* genes and PER and TIM proteins that feedback-inhibit CLK/CYC activity. CLK/CYC also activates the transcription of genes encoding VRILLE (VRI) and PDP-1, negatively and positively regulating *Clk*, forming a stabilizing loop interlocked with the core loop²². Circadian clocks are present in approximately 150

¹Department of Genetics and Evolution and Institute of Genetics and Genomics of Geneva (IGE3), University of Geneva, CH-1211 Geneva, Switzerland.

✉ e-mail: Emi.Nagoshi@unige.ch

pacemaker neurons and 1800 glia in the fly brain²³. Pacemaker neurons are classified into functionally and anatomically diverse subgroups: small and large lateral ventral neurons (s- and l-LNVs), lateral dorsal neurons (LNDs), lateral posterior neurons, and three groups of dorsal neurons (DN1s, DN2s, and DN3s). The s- and l-LNVs express the neuropeptide pigment-dispersing factor (PDF), essential for synchronizing rhythmicity across the pacemaker circuit. The PDF-positive s-LNVs (the M-cells) drive the morning peak of activity under light-dark cycles (LD) and control free-running 24-h period locomotor rhythms in constant darkness (DD)^{24,25}. The robustness and flexibility of the locomotor behavior adapting to environmental conditions require the communication between M-cells and the second set of pacemaker subtypes, the E-cells, comprising the PDF-negative fifth s-LNV, half of the LNDs, and some of the DN1s (reviewed in ref. 26). The pacemaker circuit controls circadian locomotor output and regulates brain-wide rhythmic physiology by conveying time-of-day information to different areas in the brain, such as the mushroom bodies (MBs)²⁷ and the posterior medial protocerebrum 3 (PPM3) cluster DA neurons^{28,29}.

Misalignment between environmental cycles and endogenous circadian rhythms increases the risk for physical and psychiatric disorders³⁰. Genetic and environmental disruption of circadian rhythms in flies leads to adverse health consequences, including increased mortality in response to oxidative stress³¹ and lifespan reduction³², suggesting that the mechanisms underpinning the link between circadian disruption and diseases can be studied in flies. *Clk* loss of function in the s-LNV pacemaker neurons causes loss of DA neurons in the PPL1 cluster, resulting in age-dependent locomotor decline; intriguingly, this process is PDF-dependent and circadian-clock-independent³³. Therefore, questions remain regarding whether and how the circadian system regulates the (patho-)physiology of DA neurons.

Here, we used *Drosophila* as a model to ask whether circadian clocks causally impact degenerative processes in PD. We found that DA neurons in the PAM cluster exhibit diurnal and circadian rhythms in vulnerability to oxidative stress. Loss of circadian clock genes results in age-dependent PAM neuron loss and exacerbates oxidative stress-induced PAM neuron loss. We identified PAM- α 1 neurons as one of the susceptible DA neuron subtypes and found that the circadian pacemaker circuit is presynaptic to this subgroup. Oxidative stress-induced loss of PAM- α 1 neurons leads to changes in sleep, reminiscent of PD non-motor symptoms. These findings establish a direct role of circadian clocks in controlling the timing and magnitude of the vulnerability of DA neurons.

Results

Circadian vulnerability of DA neurons to oxidative insults

We previously demonstrated that flies exposed to hydrogen peroxide (H₂O₂) or paraquat for 24 h display selective loss of DA neurons in the PAM cluster (Fig. 1a)^{12,13,21}. To evaluate dopaminergic neurodegeneration from a circadian perspective, we developed a short-term H₂O₂ treatment protocol that can be performed at six time points across the day. Seven-day-old *w¹¹¹⁸* flies were treated with H₂O₂ at various concentrations (5–20%) and durations (3–6 h), and survival of PAM neurons was assessed 7 days post-treatment by immunostaining for tyrosine hydroxylase (TH) (Supplementary Fig. S1a). From the conditions that induced PAM neuron loss, we chose 5% and 10% H₂O₂ treatment for 4 h in subsequent experiments because this duration is suitable for performing assays in a circadian fashion, and the effect does not saturate. Loss of TH-positive neurons was observed only in the PAM cluster among all DA neuron clusters following the short H₂O₂ treatment (Fig. 1b). H₂O₂ treatment in flies expressing red nuclear fluorescent protein RedStinger with the PAM neuron-specific *R58E02* GAL4 driver resulted in the reduction of RedStinger-positive cells, suggesting that oxidative insults cause loss of neurons and not merely the reduction in TH expression

(Supplementary Fig. S1b). Therefore, we focused on this group of DA neurons in subsequent studies.

To test whether the vulnerability of PAM neurons to oxidative stress is rhythmic, we next performed the short H₂O₂ treatment in a circadian fashion. Seven-day-old *w¹¹¹⁸* flies entrained to LD (12 h:12 h light-dark cycles) were exposed to 10% H₂O₂ for 4 h, following a 5-h food and water deprivation. H₂O₂ exposure was initiated at a different Zeitgeber Time (ZT) across the day, and DA neurons were analyzed 7 days post-treatment (Fig. 1c). Whereas the H₂O₂ treatment at any time caused significant PAM neuron loss compared to the water-only control, the treatment at ZT20 (8 h after lights-off) resulted in a more significant loss of PAM neurons than the other time points (Fig. 1d). The highest sensitivity at ZT20 was replicated in the assay with the 4-h 5% H₂O₂ treatment, validating its specificity (Supplementary Fig. S1c). We performed the same experiment in constant darkness (DD) to determine the role of endogenous clocks and LD cycles. Newly hatched flies were entrained for 3 days in LD and then placed in DD for the remainder of the experiment and treated with H₂O₂ on the fourth day in DD (DD4) (Fig. 1c). The treatment at CT4 (4 h after subjective lights-on) with 10% (Supplementary Fig. 1c) or 5% H₂O₂ (Supplementary Fig. S1d) caused a more significant PAM neuron loss than the other time points. These results suggest intrinsic rhythmicity in the vulnerability of PAM neurons to oxidative stress modulated by light.

To determine whether circadian clocks control the intrinsic rhythms of PAM neuron vulnerability, we next used *per* null (*per⁰*, also known as *per^o*) mutant flies carrying *white* mutation, devoid of molecular clocks. We first quantified PAM neuron counts in *per^o* with anti-TH staining and by expressing RedStinger without oxidative stress from days 1 to 14 of age. *w¹¹¹⁸* was used as a control strain. We found that *per^o* flies were born with fewer PAM neurons and displayed a marked, age-dependent loss of PAM neurons (Fig. 2a–c). The *tim* null (*tim^o*) mutants, also in *w* background, similarly displayed a reduced number of PAM neurons on day 1 and a progressive loss thereafter (Supplementary Fig. S2a). Both *per^o* and *tim^o* arrhythmic mutants displayed locomotor deficits, as reported previously^{33,34} (Supplementary Fig. S2b). These findings suggest that disruption of circadian clocks interferes with the development of DA neurons in the PAM cluster and accelerates their age-dependent degeneration.

Because a previous study reported that H₂O₂ exposure elicits a higher rate of mortality in *per^o* than in wild-type flies³⁴, we also examined the effect of various concentrations of H₂O₂ on PAM neuron survival in *per^o* flies at a single timepoint; 2.5% H₂O₂, which did not affect PAM neurons in *w¹¹¹⁸* and *Canton-S* (CS), robustly induced PAM neurodegeneration in *per^o* mutants (Fig. 2d). This finding suggests that loss of *per* null mutation enhances the vulnerability of PAM neurons to oxidative stress-induced degeneration. We next performed the circadian oxidative treatment with 5% H₂O₂ in LD and DD on *per^o* flies. The *per^o* flies treated with H₂O₂ at any timepoint showed a significant loss of PAM neurons as compared to the control group treated with water only. In LD, the treatment at ZT12 resulted in a more significant loss of PAM neurons than the other time points (Fig. 2e). In contrast, the difference among time points was abolished in DD (Fig. 2f). These findings suggest that the circadian clock gene *per* controls the magnitude and temporal variations of PAM neuron sensitivity to oxidative stress. In the absence of functional clocks, light can impose diurnal rhythms of PAM neuron vulnerability.

The circadian neural circuit controls the rhythmic vulnerability of PAM neurons

Because PAM neurons are not clock-containing cells, the rhythmic vulnerability of PAM neurons is non-cell-autonomously controlled by clocks located elsewhere. Several mechanisms might drive rhythms in non-clock-containing neurons, including the rhythmic H₂O₂ uptake by

feeding/drinking rhythms, systemic rhythmic changes in the brain environment, and the rhythmic modulation of the physiology of PAM neurons by circadian pacemaker neurons.

To test whether the differential loss of PAM neurons is caused by ingesting more H₂O₂ solution at one time than the others, we performed a feeding assay³⁵. Flies were fed with H₂O₂ or water mixed with blue food dye, which sticks to the gut and is not eliminated or digested. Then, spectrophotometry was performed on homogenized fly bodies to measure the amount of dye ingested. In LD and DD, flies displayed rhythmic feeding patterns when fed with the control solution (water

and dye), congruent with a previous study demonstrating the circadian regulation of feeding³⁶. In contrast, the feeding pattern of the 10% H₂O₂-containing solution was not rhythmic. Its uptake was significantly lower than the control solution across all time points (Fig. 3a). This finding is consistent with the finding that 2.5% H₂O₂ caused a more significant neuronal loss than the higher concentration in *per⁰* flies (Fig. 2d), probably because flies ingest more H₂O₂ solutions at lower concentrations. Therefore, daily variations in the feeding pattern do not account for the circadian vulnerability of PAM neurons. We also found that flies drink three to five times more in DD than in LD, which

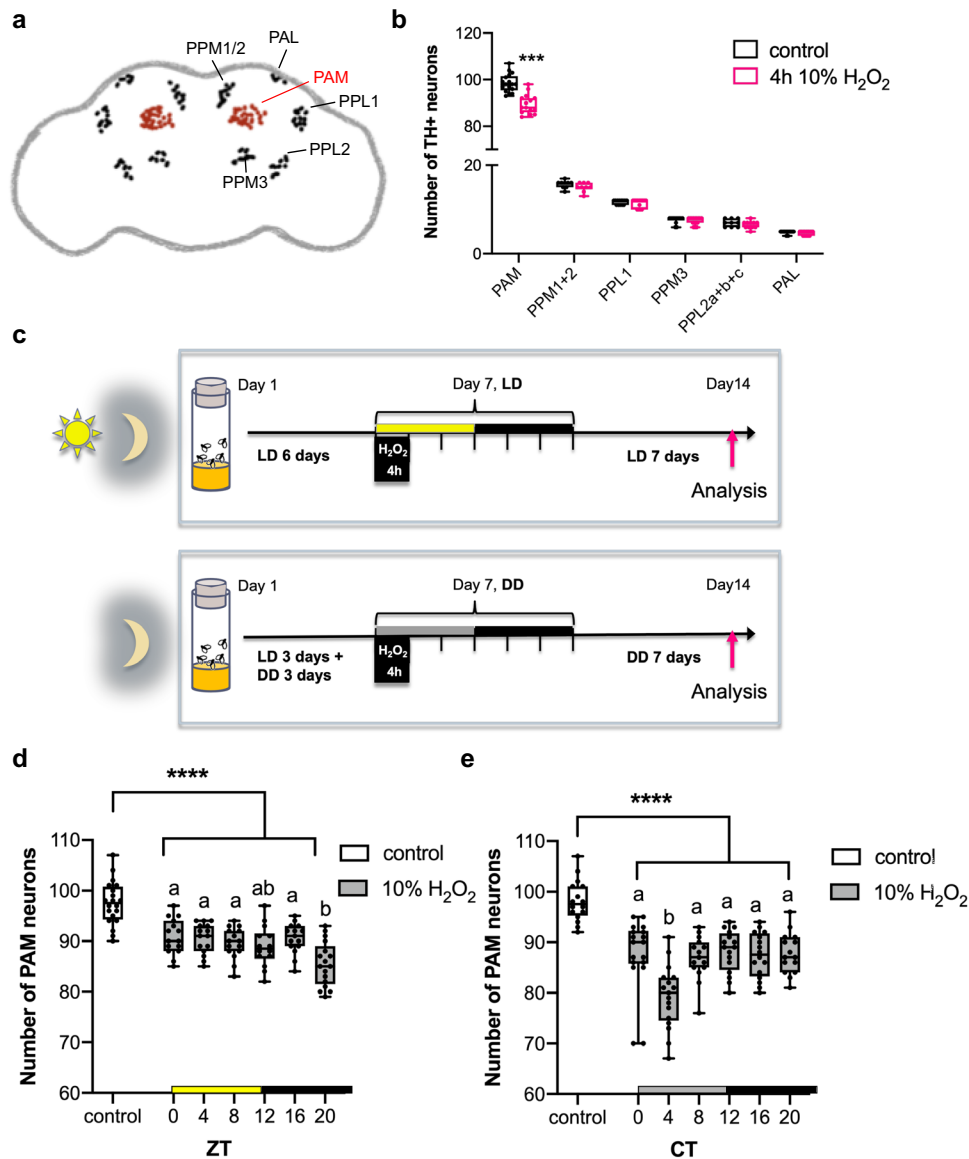
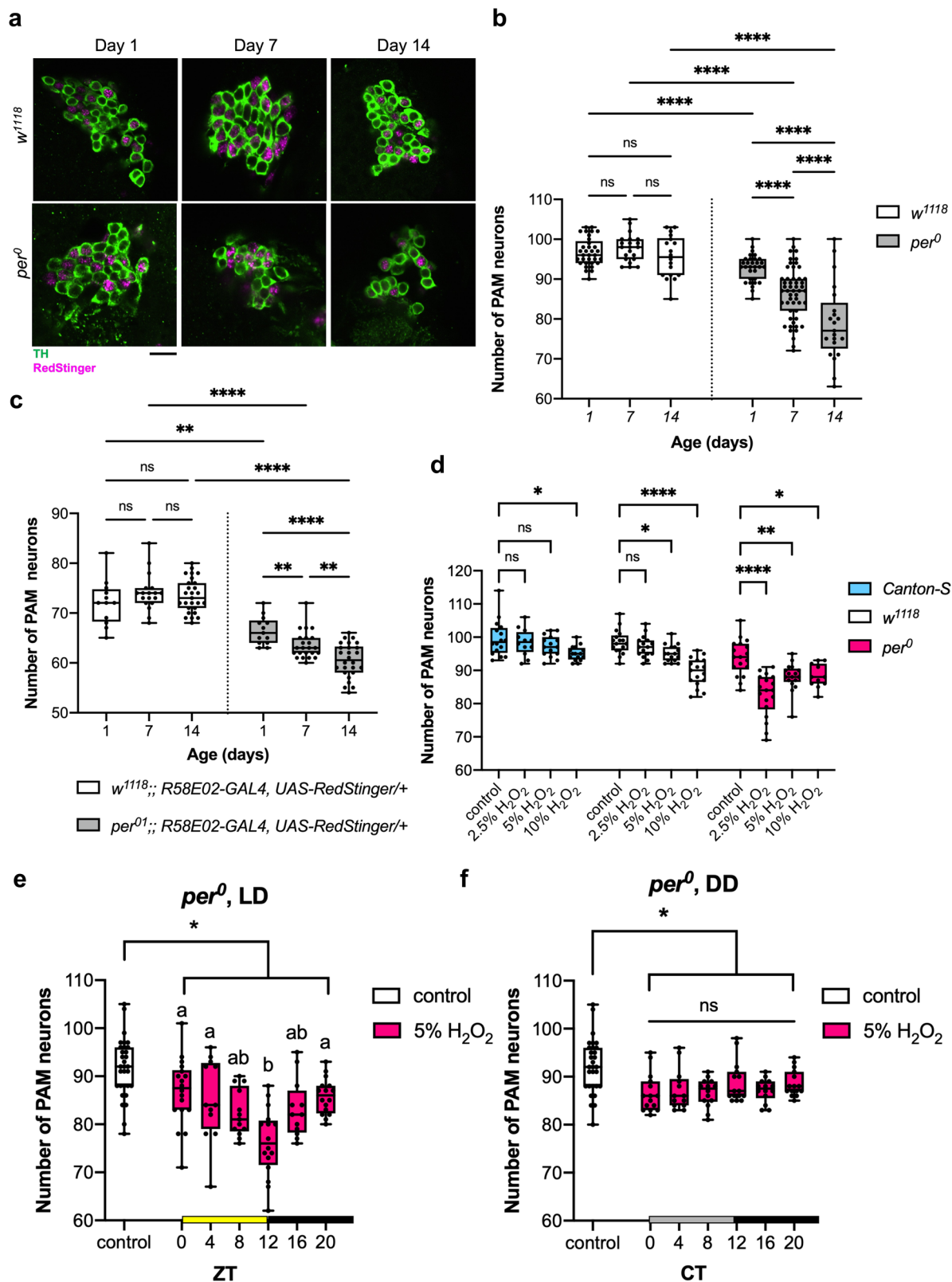


Fig. 1 | Rhythmic vulnerability of PAM neurons to oxidative stress. **a** A schematic of the cell bodies of DA neuron clusters in the adult fly brain. PAM protocerebral anterior medial, PAL protocerebral anterior lateral, PPL1 and 2 protocerebral posterior lateral 1 and 2, PPM1, 2, and 3 protocerebral posterior medial 1, 2, and 3. **b** DA neuron counts in *w¹¹¹⁸* flies per hemisphere in each cluster 7 days after a 4-h 10% H₂O₂ treatment performed at ZT20. The control group was treated with water only. DA neurons were detected by anti-TH immunostaining. Neurodegeneration was observed only in the PAM cluster following the H₂O₂ treatment ($n = 18$ hemispheres analyzed for both groups). **** $p < 0.0001$ (two-tailed t -test, comparing the control and H₂O₂-treated groups). In box plots in this and all following figures, box boundaries are the 25th and 75th percentiles, the horizontal line across the box is the median, and the whiskers indicate the minimum and maximum values. The dots represent all data points. **c** A schematic of the circadian

H₂O₂ treatment protocol. **d, e** Quantification of the number of PAM neurons after the 4-h 10% H₂O₂ treatment performed at different times in LD (control, $n = 20$; ZT0, 4, 8 and 16 $n = 15$ each; ZT12, $n = 14$; ZT16, $n = 17$ hemispheres) (**d**) or DD (control, $n = 16$; CT0, $n = 18$, CT4, $n = 17$; CT8 and 20, $n = 15$ each; CT12 and 16, $n = 16$ each) (**e**). The x -axis indicates the times when H₂O₂ was applied. The control group was treated with water only at ZT20 in LD (**d**) and CT20 in DD (**e**). At all time points, PAM neuron counts in the H₂O₂ treatment group are significantly smaller than those in the control group. **** $p < 0.0001$ (one-way ANOVA with Tukey's post hoc test). Within the H₂O₂-treated group, flies treated at ZT20 in LD (**d**) and CT4 in DD (**e**) showed significantly greater cell loss than the treatment at any other time. Different lowercase letters represent statistical significance by one-way ANOVA with Tukey's HSD post hoc test. Source data are provided as a Source Data file.



explains the more pronounced loss of PAM neurons following the H₂O₂ treatment in DD than in LD (Fig. 1d, e, Supplementary Fig. S1c, d).

The circadian H₂O₂ feeding assay requires flies to be starved before and during H₂O₂ exposure. We next tested whether the starvation and dehydration associated with the assay led to the rhythmic PAM neurodegeneration. To this end, flies were removed from food and water for 9 h, 5 h before and 4 h after ZT20. Seven

days later, PAM neurons were examined by anti-TH immune staining. The control group was given access to water for 4 h after a 5-h starvation/water deprivation period. The results showed no changes in PAM neuron count between the groups (Fig. 3b). This finding suggests that the loss of PAM neurons and their rhythmicity are not caused by starvation or dehydration before or during the H₂O₂ treatment.

Fig. 2 | The clock gene *per* controls the magnitude and rhythms of the vulnerability of PAM neurons to oxidative stress. **a** Representative maximum-projection images of PAM neurons in *w¹¹¹⁸* and *per⁰* flies at indicated ages. PAM neurons were visualized by anti-TH antibodies (green) and RedStinger driven by the *R58E02* driver (magenta). Approximately half of the neurons in the PAM cluster are visible. Scale bar, 20 μ m. **b, c** The number of PAM neurons detected by anti-TH immunostaining (*w¹¹¹⁸* day1, $n = 33$; day7, $n = 21$; day14, $n = 18$ hemispheres. *per⁰* day1, $n = 31$; day7, $n = 52$; day14, $n = 21$) (**b**) and by the expression of *R58E02*-driven RedStinger (*w¹¹¹⁸* day1, $n = 12$; day7, $n = 17$; day14, $n = 27$ hemispheres. *per⁰* day1, $n = 13$; day7, $n = 23$; day14, $n = 26$) (**c**). *per⁰* flies display developmental and age-dependent loss of PAM neurons. $^{**}p < 0.01$ and $^{****}p < 0.0001$ (two-tailed *t*-test or two-tailed Mann–Whitney U test). **d** PAM neuron counts in *Canton-S*, *w¹¹¹⁸*, and *per⁰* were assessed by anti-TH staining 7 days after the treatment with different concentrations of H₂O₂. Treatment was performed from ZT1 for 4 h. (*Canton-S* control, $n = 16$, 2.5% H₂O₂, $n = 12$; 5%, $n = 15$; 10%, $n = 16$ hemispheres. *w¹¹¹⁸* control, $n = 17$; 2.5%, $n = 16$; 5%, $n = 16$; 10%, $n = 17$. *per⁰* control, $n = 18$; 2.5%, $n = 18$; 5%, $n = 17$; 10%,

$n = 11$) *per⁰* flies display increased PAM neuron susceptibility compared to control genotypes. $^{*}p < 0.05$, $^{***}p < 0.001$, and $^{****}p < 0.0001$ (one-way ANOVA with Dunnett's multiple comparisons test). **e, f** PAM neuron counts in *per⁰* flies after a 4-h 5% H₂O₂ treatment were performed at different time points in LD (control, $n = 31$; ZT0, $n = 18$; ZT4, $n = 12$; ZT8, $n = 13$; ZT12, $n = 16$; ZT16, $n = 12$; ZT20, $n = 16$ hemispheres) (**e**) or DD (control, $n = 30$; CT0, $n = 15$; CT4, $n = 13$; CT8, $n = 14$; CT12, $n = 15$; CT16, $n = 14$; CT20, $n = 15$ hemispheres) (**f**). The x-axis indicates the time points when H₂O₂ was applied. The control group was treated with water only at ZT0 in LD (**e**) and CT0 in DD (**f**). At all time points, PAM neuron counts in the H₂O₂ treatment group were significantly smaller than those in the control group. $^{*}p < 0.05$ (one-way ANOVA with Tukey's HSD post hoc test). Within the H₂O₂-treated group, flies treated at ZT12 in LD (**e**) displayed a significantly greater cell loss than at any other time point. No difference was observed between time points in DD (**f**). Different lowercase letters represent statistical significance by one-way ANOVA with Tukey's post hoc test. Source data are provided as a Source Data file.

The results obtained so far suggest that the loss of PAM neurons can be directly attributed to the increased levels of reactive oxygen species (ROS) in PAM neurons resulting from H₂O₂ treatment rather than the systemic effects triggered by H₂O₂ ingestion. To test this further, we expressed catalase, an enzyme that breaks down H₂O₂ into water and oxygen, specifically in the PAM neurons using the *R58E02* driver. The expression of catalase effectively prevented the H₂O₂-induced loss of PAM neurons in both LD (treated at ZT20) and DD (at CT4 and CT16) (Fig. 3c, d). These results indicate that the elevation of ROS within the PAM neurons directly leads to the neurodegeneration of PAM neurons following exposure to H₂O₂.

Endogenous oxidative stress levels vary daily in flies and mammals^{31,37}. We wondered whether the rhythms in endogenous ROS levels in the fly brain and H₂O₂ administered at specific times would accumulate to trigger a rhythmic neuronal loss in the PAM cluster. To test this possibility, we used MitoSOX (a ROS-sensitive fluorescent dye targeted to mitochondria) to monitor mitochondrial ROS levels across the day in PAM neurons labeled with *R58E02>UAS-EGFP* in *w¹¹¹⁸* flies. In 7-day-old flies, MitoSOX fluorescence intensity in PAM neurons in LD showed daily variations and peaked at ZT20 (Fig. 3e), the time when PAM neurons are the most vulnerable to H₂O₂ (Fig. 1d). This finding suggests that oscillating levels of endogenous ROS combined with the H₂O₂ treatment might account for the differential loss of PAM neurons in LD. In contrast, no significant differences in MitoSOX levels were observed between time points in DD (Fig. 3e, Supplementary Fig. S3). Therefore, another mechanism under the control of circadian clocks gates the vulnerability of PAM neurons in DD.

To test whether PER-expressing clock neurons directly or indirectly modulate PAM neuron vulnerability, we re-expressed the PER protein in clock neurons in *per⁰* mutants and examined PAM neurons. Genetic rescue of *per* with the pan-clock neuron driver *Clk1982-GAL4*³⁸ significantly increased the number of PAM neurons at day 14 compared to *per⁰* without H₂O₂ treatment. Thus, the pan clock-neuron *per* rescue prevented the accelerated age-dependent loss of PAM neurons caused by loss of *per* (Fig. 4a). *Clk1982>per* also reversed the exacerbated loss of PAM neurons following H₂O₂ treatment in *per⁰* to the level of *w¹¹¹⁸* flies (Fig. 4b). These results suggest that loss of PER in clock neurons is responsible for the enhanced PAM neuron loss in *per⁰* mutants, at least in part.

To test if any subclass of clock neurons is essential for the role of PER in regulating PAM neuron survival, we next performed *per⁰* genetic rescue using *Pdf-GAL4*, expressed in the *s*- and *l*-LNvs except the fifth *s*-LNv^{39,40}, and *DvPdf-GAL4*, which targets all LNvs, three CRY-negative LNds, and one CRY/ITP double-positive LNd^{41,42}. Both rescue genotypes restored the number of PAM neurons to the level of *w¹¹¹⁸* under basal conditions (Fig. 4a). The number of surviving PAM neurons after H₂O₂ treatment was also significantly greater in both rescue genotypes than in control expressing only the driver (Fig. 4b). PER rescue with

Pdf-GAL4 or *Clk1982-GAL4* showed similar levels of protection against H₂O₂, whereas, with *DvPdf-GAL4*, the protection was partial. This might be due to differential expression levels within the LNvs between *Pdf-GAL4* and *DvPdf-GAL4*.

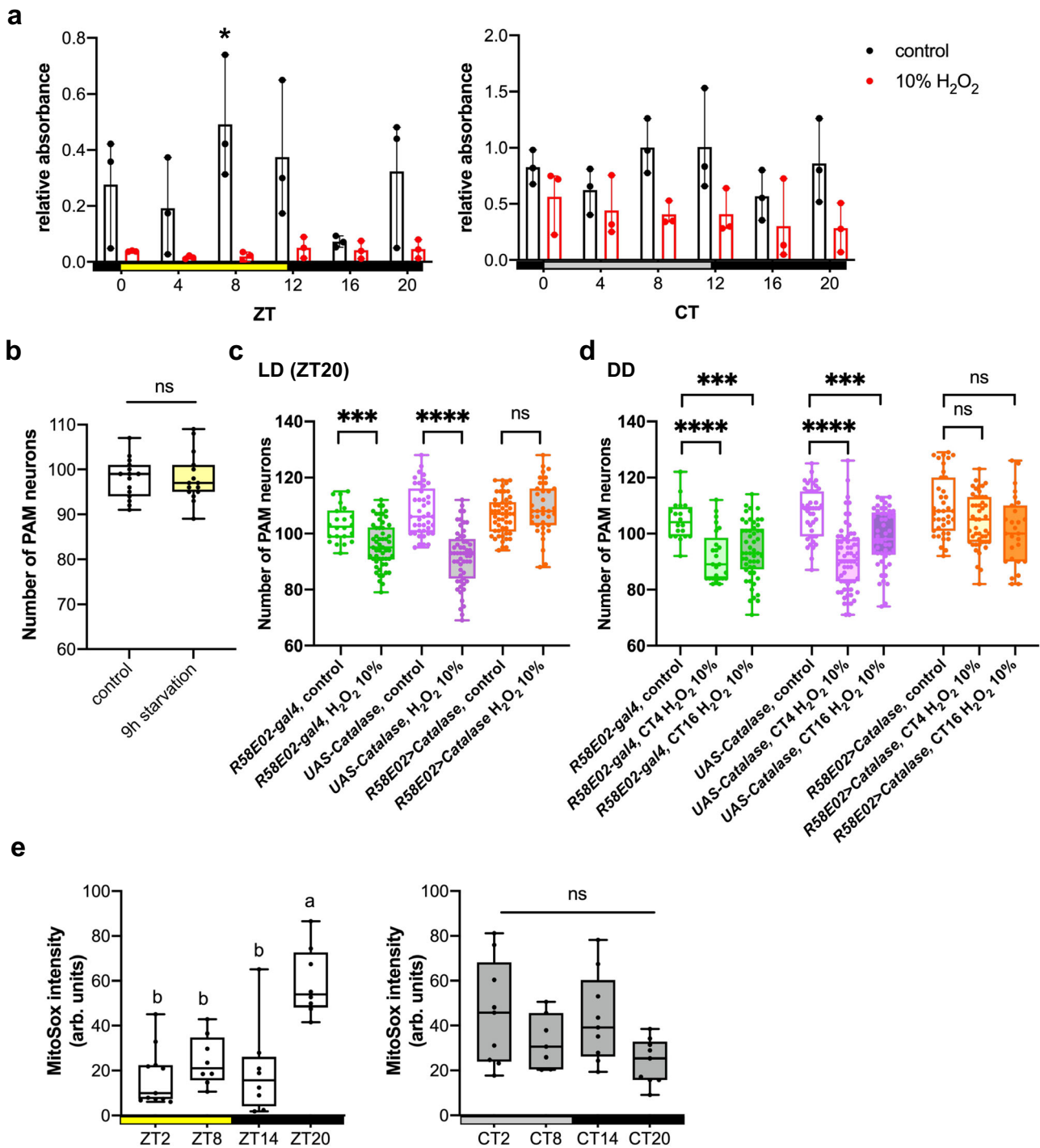
Additionally, we examined whether the genetic rescue of *per⁰* in clock neurons could prevent PAM neuron loss in DD. *Clk1982-GAL4* is highly expressed in most clock neurons, except in the LPN, but has an ectopic expression in non-clock cells, such as the Kenyon cells. Therefore, we included a second pan-clock neuron driver, *Clk856-GAL4*, which covers LPN and has a reduced ectopic expression³⁸ in this experiment. H₂O₂ treatment was performed at CT4 and CT16. The number of PAM neurons was significantly higher in all the rescue genotypes compared to *per⁰* at both time points ($^{****}p < 0.0001$ for each pairwise comparison between *per⁰* and the rescue genotypes). Flies rescued with either *Clk1982-GAL4* or *DvPdf-GAL4* exhibited partial protection against H₂O₂-induced PAM neuron loss, whereas flies rescued with *Clk856-GAL4* or *Pdf-GAL4* were completely resistant to H₂O₂ at both time points (Fig. 4c). These findings suggest that *Clk856-GAL4* and *Pdf-GAL4* may drive the expression of PER above endogenous levels, thereby bolstering the resistance of PAM neurons beyond that in wild-type flies. Taken together, these findings suggest that PER expression within the PDF-positive LNvs plays a significant role in the regulation of survival of PAM neurons following oxidative insults.

A subset of clock neurons are presynaptic to PAM neurons

The finding that PER expressed in circadian pacemaker neurons controls rhythmic PAM neuron vulnerability suggests that PAM neurons are directly or indirectly downstream of circadian neural circuits. To test this possibility, we examined postsynaptic targets of *DvPdf-GAL4*-expressing neurons using *trans-Tango*⁴³, an anterograde transsynaptic tracing tool. Several neurons in the most anterior region of the PAM cluster were marked with the postsynaptic signal, indicating the direct projection from the *DvPdf-GAL4*-labeled neurons to 6 to 7 PAM neurons (Fig. 4d). In contrast, the *trans-Tango* assay with *Pdf-GAL4* did not result in any positive signal within the PAM cluster (Fig. 4d), suggesting that the *s*- and *l*-LNv neurons are not presynaptic to PAM neurons. These findings taken together suggest that all or some *DvPdf*-positive but *Pdf*-negative cells (i.e., the three CRY-negative LNds, one CRY/ITP double-positive LNd, and the fifth LNv) are presynaptic to PAM neurons (Fig. 4e).

Identification of the vulnerable subpopulation of PAM neurons

PAM neurons are highly heterogeneous, encompassing 14 subclasses of morphologically and functionally diverse neurons projecting to different subdomains of the MB and other brain regions⁴⁴. Because the number of neurons lost following H₂O₂ treatment was relatively consistent between experiments within the same genotype, we wondered if the vulnerable neurons belong to a specific subset(s) of PAM



neurons. To test this possibility, we first used classical GAL4 drivers to label most or some PAM neurons with GFP to roughly locate the subclass vulnerable to H₂O₂ administered at ZT20. Most (8 of 13) PAM neurons that degenerated after the H₂O₂ insult belonged to the group expressing *R58E02-GAL4* (Fig. 5a).

To identify the vulnerable PAM subgroup within the *R58E02*-positive cells, we tested split-GAL4s. From the available split-GAL4 drivers created at the Janelia Research Campus⁴⁵, we selected all lines with activation domains driven with the *R58E02* promoter, i.e., MB312B, MB043B, MB299B, and MB315C. These drivers label the neurons innervating different but partly overlapping areas of the MBs: MB312B-neurons send projections to the γ -lobe (γ 4 subdomain), MB043B-neurons to the α - β -, and β '-lobes (α 1, β 1, β 1ap, and β 1m

subdomains), MB299B neurons to the α -lobe (α 1 subdomain) and MB315C-neurons to the γ -lobe (γ 5 subdomain)⁴⁴. *UAS-GFP* was expressed with each of these drivers, and the number of remaining GFP-positive cells after short-term H₂O₂ treatment was scored. Neuronal loss was observed within the clusters labeled by the MB315C and MB299B drivers (Fig. 5b, c). We tested one more split-GAL4 driver (MB441B) that does not contain the *R58E02*-driven component but is expressed in the PAM neuron subset projecting to the MB γ -lobe (γ 3 subdomain). H₂O₂ treatment caused a loss of neurons within the subpopulation labeled by MB441B (Fig. 5b, c). These results suggest that PAM neurons innervating the MB γ 3, γ 5, and α 1 subdomains (PAM γ 3, γ 5, and α 1 subgroups, respectively) are subpopulations vulnerable to neurodegeneration after oxidative insults (Fig. 5d). Of these, the

Fig. 3 | Oxidative stress elicited by H₂O₂ ingestion but neither feeding rhythms nor dehydration causes circadian vulnerability of PAM neurons. **a** Feeding patterns of *w¹¹¹⁸* flies in LD (left) and DD (right). Flies were fed for 4 h with 10% H₂O₂ solution containing blue dye. The control solution contained only water and blue food dye. *n* = 15–25 flies. The *x*-axis indicates the time points when the flies started to be fed. The *y*-axis represents the relative absorbance per ten flies. The dots represent the values of three independent experiments. Feeding levels in the control group at ZT8 were significantly higher than at other time points in LD. **p* < 0.05 in any pairwise comparison (ANOVA with Tukey's post hoc test). Error bars indicate the range. No significant difference was observed between time points in all other groups. **b** PAM neuron counts after 9 h of food and water deprivation, started at ZT15. The control group was deprived of food and water for 5 h, followed by 4 h of water access. *n* = 15 hemispheres for both groups. No significant difference between groups (*t*-test). **c, d** Catalase was expressed in PAM neurons with the *R58E02* driver, and its effect on H₂O₂-induced PAM neuron loss was assessed by

anti-TH immunostaining in LD (**c**) and DD (**d**). Catalase expression prevented PAM neuron loss following a 4-h 10% H₂O₂ treatment performed at ZT20 (**c**), as well as at CT4 and CT16 (**d**). The control group was treated with water at the same time point. ****p* < 0.001 (*p* = 0.0004 in **c**); *p* = 0.0004 between *R58E02* control and CT16 H₂O₂, *p* = 0.0006 *UAS-Catalase* control vs. CT16 H₂O₂ in (**d**) and *****p* < 0.0001 (Kruskal–Wallis test with Dunn's multiple comparisons test). In (**c**), *R58E02* control, *n* = 22; H₂O₂, *n* = 54 hemispheres. *UAS-Catalase* control, *n* = 41; H₂O₂, *n* = 55. *R58E02*>*Catalase*, *n* = 50; H₂O₂, *n* = 37. In (**d**), *R58E02* control, *n* = 20; CT4 H₂O₂, *n* = 25; CT16 H₂O₂, *n* = 52 hemispheres. *UAS-Catalase* control, *n* = 43; CT4 H₂O₂, *n* = 68; CT16 H₂O₂, *n* = 49. *R58E02*>*Catalase* control, *n* = 39; CT4 H₂O₂, *n* = 47; CT16 H₂O₂, *n* = 27. **e** ROS levels within the PAM neurons were measured using MitoSOX red in flies expressing *EGFP* with the *R58E02* driver in LD (left) and DD (right). ZT2, *n* = 11; ZT 8, 14 and 20; 8 flies. CT2, 14 and 20, *n* = 9; CT8, *n* = 7. ROS levels are significantly elevated at ZT20 in LD but do not differ among time points in DD (ANOVA with Tukey's post hoc test). Source data are provided as a Source Data file.

PAM α 1 subgroup labeled by MB299B was the most vulnerable, as more than 50% degenerated after the H₂O₂ treatment (Fig. 5b–d).

We next determined whether these PAM subpopulations were rhythmically vulnerable to oxidative stress, focusing on the most vulnerable MB299B-labeled neurons (PAM- α 1). We treated 7-day-old flies expressing GFP with the MB299B split-GAL4 at ZT8 and ZT20 with 10% H₂O₂, and the GFP-positive cell count was scored 7 days later. The H₂O₂ treatment at ZT8 caused the loss of around three to four neurons, whereas, on average, 7 neurons were lost from the treatment at ZT20. Thus, PAM- α 1 indeed shows rhythmicity in vulnerability to oxidative stress, at least in LD (Fig. 5e, f). In DD, exposure to H₂O₂ at CT4 and CT16 both induced a significant loss of the MB299B-labeled neurons, but no difference between time points was observed (Fig. 5g). This finding suggests the presence of another PAM subpopulation that displays rhythmic vulnerability in DD.

We also analyzed the *Janelia* Research Campus hemibrain connectome data⁴⁶, which were visualized using the NeuPrint interface⁴⁷ to assess the structural connectivity between clock neurons and MB299B neurons. Although chemical synapses between the LNvs or LNds and PAM- α 1 neurons are not annotated in the hemibrain data set⁴⁶, visual inspection using the NeuPrint tool revealed close contacts between the axonal projections of the LNds and MB299B neurons (Fig. 6a), whereas projections of the s-LNvs and MB299B neurons did not show apparent contacts (Supplementary Fig. S4a). These findings are consistent with the results of the *trans*-Tango experiment (Fig. 4d) and suggest that input from the LNds modulates the vulnerability of MB299B neurons in a circadian fashion. We found that the projections of the LNds also contacted MB315C and MB441 neurons, supporting the notion that vulnerable PAM neuron subsets are postsynaptic to the LNds (Supplementary Fig. S4b, c).

Rhythmically vulnerable PAM subpopulations exhibit calcium rhythms

The finding that MB299B-positive, PAM- α 1 neurons are rhythmically vulnerable to oxidative insults in LD and postsynaptic to LNds raises the possibility that they exhibit physiological rhythms. Therefore, we measured levels of intracellular Ca²⁺, a second messenger that controls several cellular functions, in PAM- α 1 neurons across 24 h in live flies (Fig. 6b). The calcium sensor GCaMP7s⁴⁸ was expressed with the MB299B driver, and the 3-day-old flies were entrained to LD cycles for four days before imaging in DD. Ca²⁺ levels in these neurons showed temporal variations, with peaks twice a day, around CT5 and CT17 (Fig. 6c). In *per⁰* flies, GCaMP fluorescence levels were uneven across time points, and the bimodal pattern in *w¹¹¹⁸* was lost, with a peak around CT17 (Fig. 6d). These results suggest that circadian inputs to the PAM- α 1 neurons rhythmically modulate their activity that peaks just before midday and before midnight.

We next wanted to know whether decreased excitability could be neuroprotective. Therefore, we silenced PAM neurons by

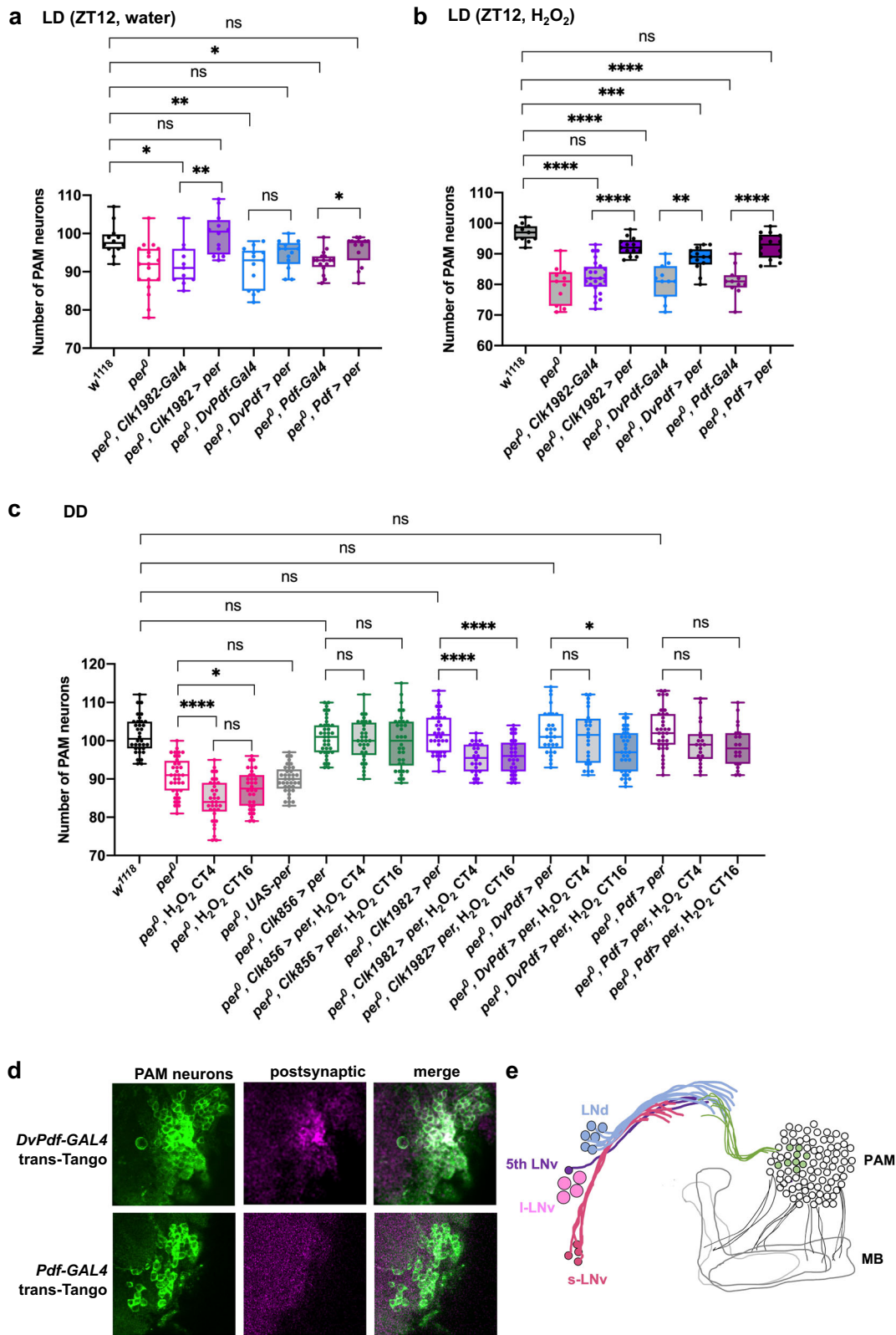
overexpressing the inward rectifier K⁺ channel, Kir2.1⁴⁹, with the *R58E02* driver and tested whether this silencing prevents the degeneration of PAM neurons after the oxidative stress challenge. However, significantly fewer PAM neurons were present in the 14-day-old flies expressing Kir2.1 than in the control without H₂O₂ treatment, probably due to developmental impairments. Moreover, Kir2.1 overexpression did not prevent H₂O₂-induced PAM neuron loss (Supplementary Fig. S5). This finding suggests that neuronal activity levels are unlikely to be the cause of the selective and rhythmic vulnerability of PAM- α 1 neurons.

Consequences of PAM- α 1 neurodegeneration on motor and non-motor functions

Four-hour treatment with 10% H₂O₂ at ZT20 leads to the loss of approximately 13 DA neurons in the PAM cluster, most of which belong to the PAM- α 1 subclass (Fig. 5a–d). We wondered whether this loss of approximately 10% of PAM neurons would have immediate or long-term effects on motor or non-motor functions. It was reported that synaptic dysfunction of a small subset of PAM neurons (expressing *NP6510-GAL4*) could impair the fly's ability to climb¹⁴. To test whether the PAM- α 1 subgroup has a similar role in climbing ability, we performed a startle-induced negative geotaxis assay²¹ after the short-term H₂O₂ treatment with increasing age. Climbing abilities of control and treated flies declined with age, as expected and as previously reported¹⁴. However, there was no difference between the control and experimental groups up to day 56, i.e., 49 days post-H₂O₂ treatment (Supplementary Fig. S6), except for day 49. These findings suggest that PAM- α 1 is not involved in the control of climbing behavior.

DA neurons play various roles in regulating behavior and physiology, including sleep. Dopaminergic input to the MB regulates several aspects of sleep⁵⁰. Because the role of the MB α 1 compartment on sleep remains elusive, we next examined the effect of H₂O₂-induced loss of PAM- α 1 on sleep. Following the short-term H₂O₂ treatment on day 7 in LD, flies were maintained under LD cycles, and sleep was analyzed over 3 days starting at days 11 and 17. The results showed an increase in total sleep duration in H₂O₂-treated flies in both age groups (Fig. 7a, b). Whereas total sleep duration was increased both during the day and the night, mean sleep episode duration was increased after the H₂O₂ treatment only during the night, indicating that consolidation of sleep occurred specifically during the night. This effect was more pronounced in older flies (Fig. 7c, d). In contrast, activity levels of the flies during the waking period were not different between the H₂O₂-treated and non-treated groups at both ages (Fig. 7e, f). These findings indicate that a 4-h H₂O₂ treatment increases sleep but not hypoactivity.

H₂O₂ administration may affect sleep independently of its effect on PAM- α 1 neurons. To distinguish these possibilities, we measured sleep while blocking the output of PAM- α 1 neurons using a temperature-sensitive mutant of dynamin, *Shibire^{ts}* (*Shi^{ts}*). *UAS-Shi^{ts}*



was driven with MB299B, and sleep and activity were monitored under 30 °C between day 11 and 13 after eclosion in flies that were raised at 19 °C. In comparison to control flies carrying only *UAS-Shi^{TS}*, *MB299B>Shi^{TS}* flies showed an increase and decrease in total sleep duration during the day and the night, respectively (Supplementary Fig. S7a). Sleep was more consolidated during the day (Supplementary Fig. S7b); however, the mean activity count during the waking period

was reduced across 24 h, indicating hypoactivity (Supplementary Fig. S7c). Thus, inhibition of PAM- α 1 synaptic output not only reduces activity levels but also modulates sleep. Although the effect on sleep by H₂O₂ exposure and synaptic block are not identical, possibly due to the temperature difference and the incomplete blockage of neuropeptide release by *Shi^{TS1,52}*, these results collectively suggest the involvement of PAM- α 1 neurons in the regulation of sleep and activity. However, it

Fig. 4 | PER expression in clock neurons preserves PAM neurons. **a–c** Genetic rescue of *per* in clock neurons in *per⁰* mutants. PAM neurons were counted using anti-TH staining 7 days after a control treatment with water (**a**) and after a 4-h treatment with 2.5% H₂O₂ performed at ZT12 in LD (**b**). In (**c**), the control group was treated with water at CT16, and 2.5% H₂O₂ treatment was performed at CT4 and CT16. Genotypes are indicated on the x-axis. **a > b** represents that UAS-transgene **b** is driven by the GAL4 driver **a**. $n = 11–24$ hemispheres (see Source Data for individual sample numbers). Rescue genotypes significantly improve the preservation of PAM neurons after the H₂O₂ treatment. * $p < 0.05$, ** $p < 0.01$, *** $p < 0.001$, and **** $p < 0.0001$ (one-way ANOVA with Dunnett's multiple comparisons test, or Kruskal–Wallis test with Dunn's multiple comparisons test). All the rescue genotypes in (**c**) exhibit a significantly higher number of PAM neurons compared to *per⁰*

(**** $p < 0.0001$ for each pairwise comparison, not shown in the figure for clarity). $n = 11–19$ (**a**), $n = 11–24$ (**b**), and $n = 20–39$ hemispheres (**c**). **d** *trans*-Tango experiments using *DvPdf-GAL4* and *Pdf-GAL4* combined with TH immunostaining (green). Several postsynaptic targets of *DvPdf* neurons (magenta) were identified as PAM neurons, whereas no postsynaptic signal of *Pdf* neurons was found within the PAM cluster. Presynaptic signals by *DvPdf-GAL4* and *Pdf-GAL4* are not visible in these pictures. Two independent experiments. Scale bar, 20 μm . **e** A schematic representation of the *trans*-Tango labeling results. Projections of the l-LNVs are not shown for clarity. *DvPdf-GAL4*-positive but *Pdf-GAL4*-negative neurons, i.e., LNDs, are presynaptic to a subset of PAM neurons. Source data are provided as a Source Data file.

remains to be determined if the effects on sleep by the H₂O₂ treatment result from the loss of PAM- $\alpha 1$ neurons.

The implication of the multiple-hit hypothesis for Parkinson's disease

PD arises from the interaction of genetic and environmental risk factors and age. This notion, formulated as the multiple-hit hypothesis⁵³, suggests that short-term H₂O₂ treatment is merely a single “hit” to the dopaminergic system. To test this idea, we quantified the number of PAM neurons in the H₂O₂-treated flies over the course of aging. The difference between the control and treated groups was significant 7 days after H₂O₂ treatment and was maintained at least up to day 56 (49 days post-treatment), with no acceleration of neurodegeneration in either of the two groups (Fig. 8a).

These findings support the multiple-hit hypothesis and suggest that an insult in addition to H₂O₂ might accelerate PAM neurodegeneration. We speculated that *per⁰* mutation might constitute the second “hit,” following our finding that *per⁰* mutants display age-dependent PAM neurodegeneration (Fig. 2a–c). Therefore, we counted the number of PAM neurons over the course of aging in *per⁰* flies after the H₂O₂ treatment. On day 14, *per⁰* showed a substantial loss of PAM neurons as expected; however, after that, the rate of PAM neurodegeneration in the H₂O₂-treated flies was not higher than in non-treated flies, reaching the same number of PAM neurons on day 28 (Fig. 8b).

Increased mortality is a characteristic of PD patients⁵⁴. We monitored the life spans of *w¹¹¹⁸* and *per⁰* flies with and without H₂O₂ treatment. Whereas the H₂O₂ treatment did not affect the life spans of *w¹¹¹⁸* flies, H₂O₂-treated *per⁰* flies exhibited a significantly reduced lifespan compared to the control group (Fig. 8c, d). These results demonstrate that the combination of an oxidative insult and the *per* null mutation causes premature death of the animal.

Discussion

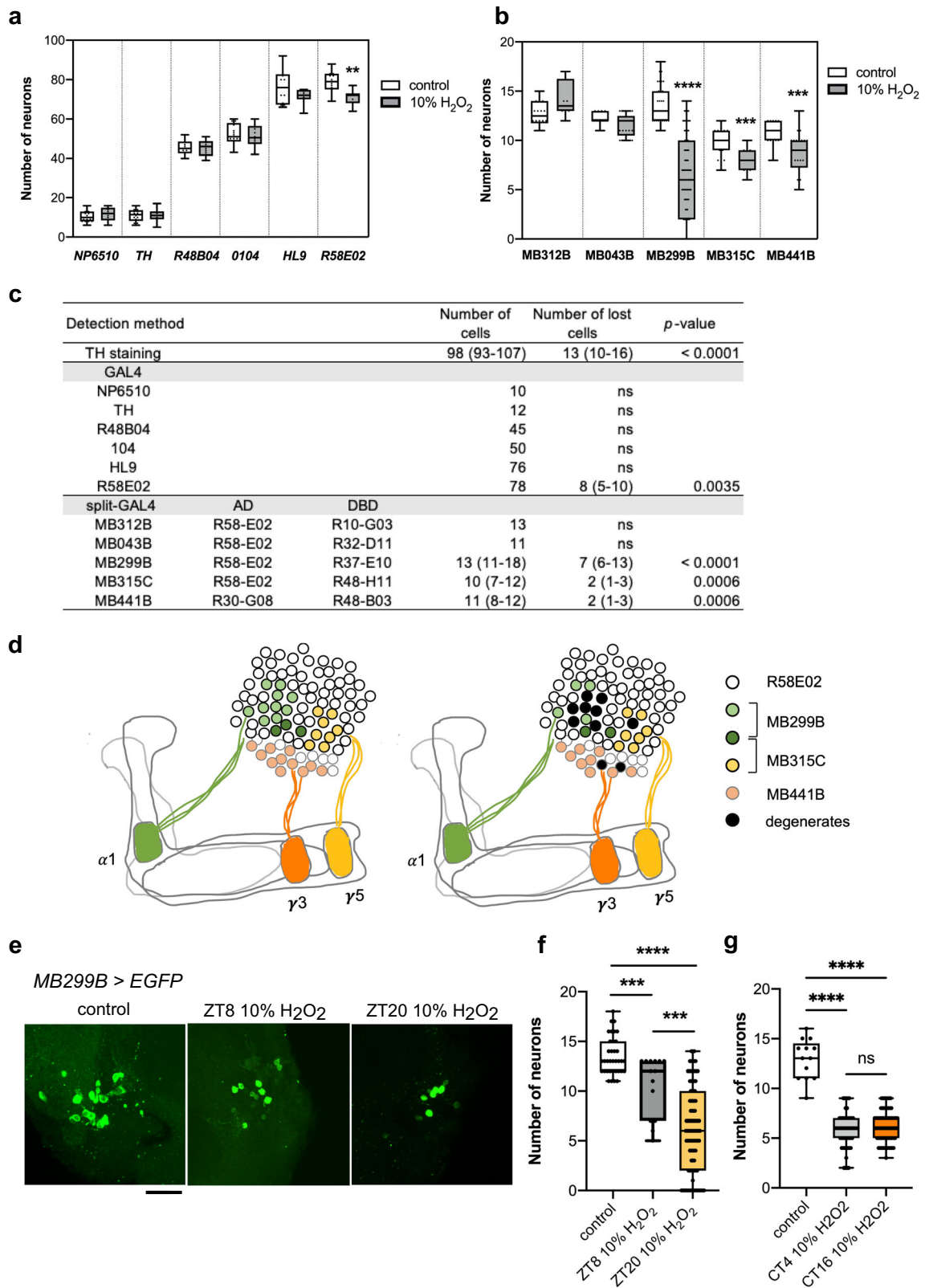
Circadian rhythm disruptions are frequent comorbidities in neurodegenerative disorders; nevertheless, little is known about how circadian clocks and neurodegeneration are causally related. Here we showed that the circadian clock gene *per* controls daily rhythms and the magnitude of the vulnerability of DA neurons to oxidative insults in *Drosophila*. The circadian pacemaker circuit is presynaptic to the vulnerable subpopulation of DA neurons, PAM- $\alpha 1$, and rhythmically modulates its intracellular Ca²⁺ levels. Oxidative stress-induced dopaminergic neurodegeneration leads to persistent changes in sleep and, combined with the *per* null mutation, causes premature death of the animal. Taken together with the finding that *per* null mutation drives progressive loss of DA neurons, our results suggest a causal role of circadian clocks in dopaminergic neurodegeneration.

PAM- $\alpha 1$ neurons are highly vulnerable and rhythmically susceptible to oxidative stress. What makes this subpopulation more susceptible than other DA neurons and how circadian inputs gate the vulnerability remain questions for future studies. The LND clock neurons are presynaptic to PAM- $\alpha 1$ neurons, and the latter exhibit *per*-dependent intracellular Ca²⁺ rhythms. Because Ca²⁺ levels in neuronal

cell bodies can be correlated with firing frequency⁵⁵, one can speculate that neuronal activity rhythms gated by the pacemaker circuit temporally regulate the vulnerability of PAM- $\alpha 1$. However, constant hyperpolarization by the expression of the Kir2.1 channel did not prevent H₂O₂-induced PAM neuron loss. The LNDs express the neuropeptide ion transport peptide (ITP), the short neuropeptide F (sNPF), and acetylcholine (Ach)⁵⁶. The neuromodulatory input by the inhibitory sNPF⁵⁷ or ITP, rather than the excitatory Ach, likely regulates the vulnerability of PAM neurons, given that neuronal silencing does not prevent PAM neuron loss. Identifying molecular differences between PAM- $\alpha 1$ and other subpopulations and potential molecular rhythmicity within PAM- $\alpha 1$ will be necessary to understand the mechanisms underlying these neurons' selective and rhythmic vulnerability. Of note, PAM- $\alpha 1$ neurons exhibit rhythmic susceptibility to H₂O₂ in LD, while no rhythms in vulnerability were observed in DD. These findings suggest the presence of another subgroup of PAM neurons that exhibit vulnerability rhythms peaking at CT4. Future studies aimed at characterizing rhythms in distinct PAM subpopulations will provide further insights into this phenomenon.

Ca²⁺ rhythms in MB299B-labeled neurons are bimodal, peaking around CT5 and CT17. This observation can be interpreted in two ways: all MB299B neurons exhibit bimodal Ca²⁺ rhythms, or there are two populations of neurons within the MB299B-labeled neurons that are anti-phasic to one another. The former possibility is reminiscent of a previous finding that the M- and E- cells of the circadian circuit²⁹ drive bimodal Ca²⁺ rhythms in the PPM3 cluster of DA neurons. The latter possibility gains support from the fact that, although PAM- $\alpha 1$ is the primary subtype labeled with the MB299B driver, weak expression of MB299B was also detected in PAM- $\beta 1$ and $\beta 2$ neurons^{17,58}. Curiously, Ca²⁺ levels in the MB299B neurons in *per⁰* show temporal variation with a peak around CT17, although its pattern is irregular and dissimilar to that of the *w¹¹¹⁸* flies. What causes this variation is unknown, but the CT17 peak might be an after-effect of the LD entrainment. Although further studies are required to untangle these issues, our observation is nevertheless consistent with the notion of connectivity between the circadian system and PAM neurons. Interestingly, the connectome data and results of the *trans*-Tango experiments suggest that the LNDs are directly connected to the MB299B-labeled neurons but not the s-LNVs. However, restoring *per* expression within the PDF-positive LNVs is sufficient to reverse the PAM neuron loss in the basal conditions and under oxidative stress in *per⁰* mutants. Because PDF-positive s-LNVs can synchronize the LNDs through PDF/PDFR signaling⁵⁹, these results suggest that the presence of PER within the PDF-positive s-LNVs is sufficient to convey a protective signal to the MB299B neurons via LNDs.

Arrhythmic *per⁰* and *tim⁰* mutants display age-dependent loss of PAM neurons. Although both mutants completely disrupt molecular clocks, the observed phenotype could be a gene-specific effect rather than the result of loss of circadian clocks per se. A previous study demonstrated that *Clk* deficiency within the s-LNVs causes age-dependent loss of DA neurons in the PPL1 cluster and accelerates locomotor decline; however, the other clock gene loss-of-function



mutants did not show the same phenotype³³. Thus, the *Clk* has a role in preventing DA neuron loss and locomotor deficits in a circadian clock-independent manner³³. Clock-independent roles of *tim* and *per* genes in mitochondrial uncoupling and lifespan have also been reported⁶⁰. It is worth noting that MB299B neurons are not the first to degenerate in the basal conditions in *per*⁰ at least up to day 7, as these neurons are present at the age when Ca²⁺ imaging was performed. These findings

underscore that clock genes play multiple roles in dopaminergic neuroprotection and are consistent with the notion that circadian disruptions are frequently comorbid with PD.

Short-term H₂O₂ treatment causes persistent increases in nighttime sleep but not locomotor defects. Blocking synaptic output of PAM- α neurons using *Shr^{TS}* increases daytime sleep and also decreases activity levels. Although sleep phenotypes observed in these two

Fig. 5 | Identification of the vulnerable subpopulations of PAM neurons.

a, b Quantification of the number of neurons labeled by GFP driven with different PAM neuron drivers, 7 days after a 4-h 10% H₂O₂ treatment at ZT20. The controls were treated with water only. **a** *UAS-EGFP* was driven with classical *GAL4* drivers as indicated in the *x*-axis. Among the drivers tested, only the *R58E02*-labeled neurons include a subpopulation vulnerable to oxidative insults. ***p* = 0.035 (two-tailed *t*-test). *n* = 7–25 hemispheres (see Source Data for individual sample numbers). **b** PAM subpopulations were labeled with split-*GAL4* drivers. Neurons labeled by MB299B, MB441B, and MB315C contain vulnerable PAM subpopulations. ****p* < 0.001 (*p* = 0.0009 MB441B control vs. H₂O₂; *p* = 0.0004 MB315C control vs. H₂O₂) and *****p* < 0.0001 (two-tailed *t*-test). *n* = 8–98 hemispheres (see Source Data for individual sample numbers). **c** Summary of the results from (a) and (b). The mean number of cells labeled by the given driver and of cells lost following the H₂O₂ treatment are shown. The numbers in the brackets indicate the range of values. AD activation domain, DBD DNA-binding domain. **d** Schematic representation of PAM subpopulations vulnerable to oxidative stress. PAM-α1, γ5, and γ3 neurons are

labeled by MB299B, MB315C, and MB441B, respectively, with three PAM-α1 neurons co-expressing MB299B and MB315C (left). H₂O₂ treatment selectively degenerates approximately half of the PAM-α1 neurons and a few cells each from the PAM-γ5 and γ3 subgroups (right). **e, f** 4-h 10% H₂O₂ treatment was performed at ZT8 and ZT20, and the number of MB299B-positive neurons was quantified 7 days post-treatment. **e** Representative confocal images of MB299B>EGFP neurons. Scale bar, 20 μm. **f** Both experimental groups have significantly fewer remaining neurons than the control group treated with water only at ZT20. H₂O₂ treatment at ZT20 caused a greater loss of neurons than at ZT8. ****p* < 0.001 (*p* = 0.0001 control vs. ZT8 H₂O₂; *p* = 0.0003 ZT8 vs. ZT20 H₂O₂) and *****p* < 0.0001 (two-tailed *t*-test). Control, *n* = 37; ZT20 H₂O₂, *n* = 98, ZT8 H₂O₂, *n* = 14 hemispheres. **g** In DD, 10% H₂O₂ treatment performed at CT4 and CT16 both led to a significant loss of MB299B neurons compared to the water-only control treatment at CT4. *****p* < 0.0001 (two-tailed Mann–Whitney test). The number of remaining MB299B neurons was similar between CT4 and CT16 treatments. Control, *n* = 13; CT4 H₂O₂, *n* = 55, CT16 H₂O₂, *n* = 71 hemispheres. Source data are provided as a Source Data file.

experiments are not identical, the results collectively point to a role for PAM-α1 neurons in sleep regulation (without excluding other PAM subpopulations). Consistent with our finding, a previous study has shown that activation of PAM neurons reduces sleep⁶¹. Lack of locomotor defects was expected, as another PAM neuron subset projecting to the MB β lobe is known to control startle-induced climbing ability¹⁴. It is well established that PAM-α1 neurons play an essential role in the acquisition and consolidation of appetitive long-term memory^{17,62} and the formation of courtship conditioning memory, which is a type of short-term memory⁵⁸. Our findings that the circadian pacemaker circuit controls these neurons raise the possibility that these learning/memory performance types may show rhythmic variations across the day. Previous studies have indeed reported such phenomena^{63,64}, albeit with some disputes⁶⁵. Moreover, because they are highly susceptible to oxidative stress-induced degeneration, their learning/memory functioning may be affected by oxidative stressors and are likely to be impaired when PAM-α1 undergoes degeneration. Thus, the circuitry involving LND–PAM-α1–MB α1 subdomain has overlapping roles in sleep and learning/memory and is susceptible to oxidative stress. Impairments in this pathway might elicit phenotypes that are reminiscent of non-motor symptoms of PD.

Several lines of evidence support the multiple-hit hypothesis for PD, suggesting that progressive PD pathology is triggered by the interaction of multiple genetic/environmental risk factors⁵³. Our finding that a single H₂O₂ treatment triggers DA neuron loss but that the rate of degeneration after that is not higher than the natural age-dependent loss in non-treated flies is consistent with the theory. We could not determine whether H₂O₂ treatment on *per*⁰ accelerates dopaminergic neurodegeneration, as this combination causes premature death. Of note, whereas immediate lethality has been reported when flies were treated with much lower concentrations of H₂O₂³¹, we did not detect any such effect. Differences in a laboratory environment or fly strains might have caused this discrepancy. If not treated, PD presents a higher mortality risk, including sudden unexpected death⁶⁶. Our findings are consistent with the multiple-hit hypothesis and suggest that genetic variations in circadian clock genes might represent a risk factor for dopaminergic neurodegeneration. We also demonstrated that an oxidative stressor administered at a specific time of day could have a critical impact on the survival of DA neurons and cause persistent changes in behavior; these findings might also be relevant in humans.

Methods

Drosophila strains and culture

Flies were reared in 12-h LD cycles in a humidified chamber at 25 °C on a standard corn meal medium. *Clk856-GAL4*³⁸ was a gift from Ralf Stanewsky. The following lines were previously described: *HL9-GAL4*⁶⁷, *R58E02-GAL*¹⁶, *per*⁰¹, *w*⁶⁸, *w;tim*⁰¹⁶⁹, *Pdf-GAL4*⁷⁰, *Clk1982-GAL4*³⁸, *DvPdf*

*GAL4*⁴¹ *UAS-per16*⁷¹, and *UAS-Shibire*¹⁵⁷². *NP6510-GAL4* (113956) was obtained from the Kyoto Stock Center. The following lines were obtained from the Bloomington Stock Center: *TH-GAL4* (Stock number 8848), *R48B04-GAL4* (50347), *O104-GAL4* (62639), *MB312B* (68314), *MBO43B* (68304), *MB299B* (68310), *MB441B* (68251), *MB315C* (68316), *UAS-GCaMP7s* (79032), *UAS-Kir2.1* (6596), *UAS-Catalase* (24621), *w*¹¹¹⁸ (5905), *Canton-S* (64349), *UAS-myrGFP*, *QUAS-mtdTomato(3xHA)*, and *trans-Tango* (77124).

H₂O₂ treatment

Male flies were collected after hatching and entrained to 12 h/12 h-LD cycles in an incubator at 25 °C. Seven-day-old flies were transferred to an empty vial for 5 h, and then a filter paper soaked with 100 μl H₂O₂ (Sigma Aldrich, 216763) of a given concentration or H₂O was inserted in the vial for a defined duration. Flies were then placed in a vial containing standard corn meal agar food for 7 days before the analysis of DA neuron integrity. For circadian H₂O₂ treatment in LD, newly hatched flies were entrained to LD cycles, and on day 7, flies were treated with 5% or 10% H₂O₂ for 4 h at one of the 6 ZT time points (ZT0, 4, 8, 12, 16 and 20) following a 5-h food and water deprivation. After the H₂O₂ exposure, flies were placed in the vial with the standard food and maintained under LD cycles at 25 °C for 7 days. For circadian treatment in DD, newly hatched flies were entrained to LD cycles for 3 days and then released to DD. After three DD cycles, flies were treated with H₂O₂ at one of the CT time points (CT0, 4, 8, 12, 16 and 20), as described above. Treatment and subsequent incubation were performed in DD.

Immunohistochemistry

Immunostaining was performed on whole fly brains. Flies were decapitated, and the whole heads were fixed in 4% paraformaldehyde + 0.3% Triton X-100 on ice for 1 h. The heads were washed with 0.3% Triton X-100 in phosphate-buffered saline (PBT) three times at room temperature. The head cuticles were partly opened, and the heads were incubated in a blocking solution (5% normal goat serum in PBT) for 1 h at room temperature. The incubation with primary antibodies was performed over two nights at 4 °C. Then, the heads were washed three times and incubated overnight with secondary antibodies at 4 °C. After three washes, the brains were dissected entirely by removing the remaining cuticle and trachea and mounted in Vectashield mounting medium (Vector laboratories, H-1000-10). The slides were stored at 4 °C and protected from light until imaging. The primary antibodies and the concentrations were as follows: rabbit polyclonal anti-TH (Millipore, ab152) 1:100; mouse monoclonal antibody nc82 (Developmental Studies Hybridoma Bank) 1:100; polyclonal rabbit anti-GFP (Invitrogen, A6455) 1:500; and monoclonal mouse anti-HA (Covance, MMS-101P) 1:200. The secondary antibodies and their concentrations were as follows: Alexa Fluor anti-rabbit 488 (ThermoFisher, A21052) 1:250 and Alexa Fluor anti-mouse 633 (ThermoFisher, A11008) 1:250.

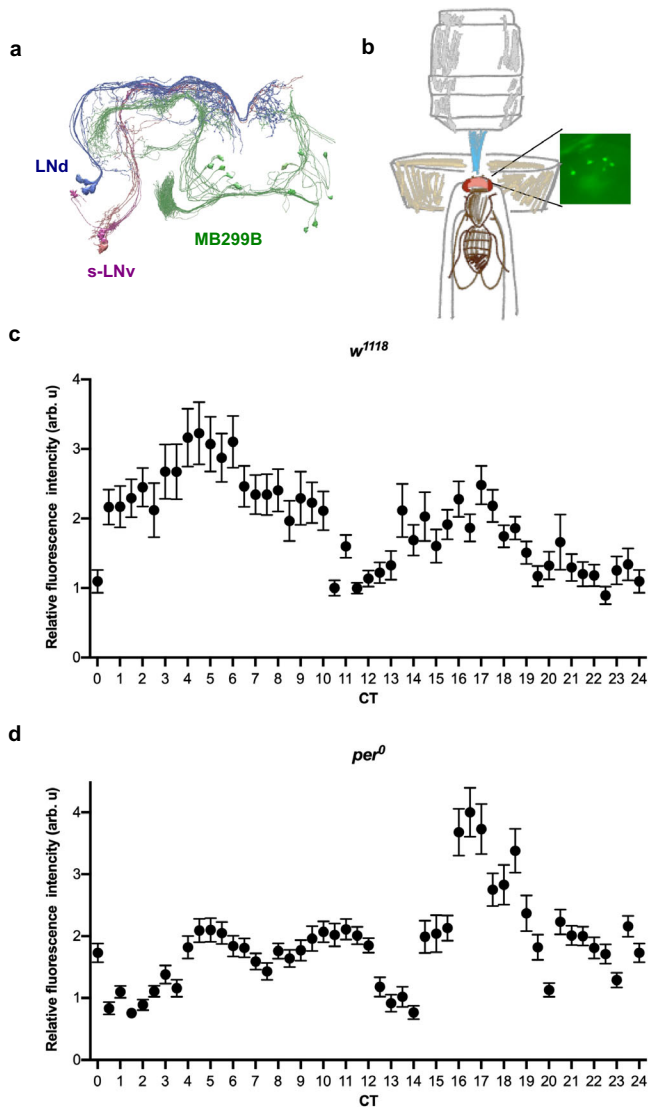


Fig. 6 | MB299B neurons display Ca²⁺ rhythms. **a** Projections of the LNDs contact dendritic arbors of MB299B neurons. Image created using the hemibrain connectome data¹⁶ via the NeuPrint tool¹⁷. **b** Illustration of the method for live GCaMP imaging. **c, d** MB299B >GCaMP7s fluorescence levels in MB299B neurons throughout 24 h on the first day in DD following LD-entrainment in *w¹¹¹⁸* (**c**) and *per⁰* (**d**). Relative fluorescence intensity (mean ± SEM) was determined from three independent experiments. In (**c**), the analysis included an average of 79 (53–146 cells) cells per timepoint from 5–10 *w¹¹¹⁸* flies (see Source Data for individual sample numbers per timepoint). In (**d**), an average of 76 (44–131) cells per timepoint from 5–10 *per⁰* flies were analyzed (see Source Data for individual sample numbers per timepoint). Source data are provided as a Source Data file.

Feeding assay

The feeding assay was performed as previously described with minor modifications³⁵. Male flies were starved for 5 h before the assay (beginning of feeding). A filter paper soaked with a 0.125 mg/ml solution of Brilliant Blue FCF was then inserted in the vial for a control group. In the vial containing the flies of the experimental group, a filter paper soaked with a 0.125 mg/ml solution of Brilliant Blue FCF with 10% H₂O₂ was inserted. The filter paper was kept in the vials for 4 h, after which the flies were flash-frozen in liquid nitrogen. Then, the flies were vortexed to detach their heads from bodies. A standard sieve (No. 25) was used to remove heads, and the bodies were transferred to 1.5-ml Eppendorf tubes. The bodies were homogenized with a motorized pestle in 1 ml of PBT and centrifuged at 13,000 rpm for 15 min to

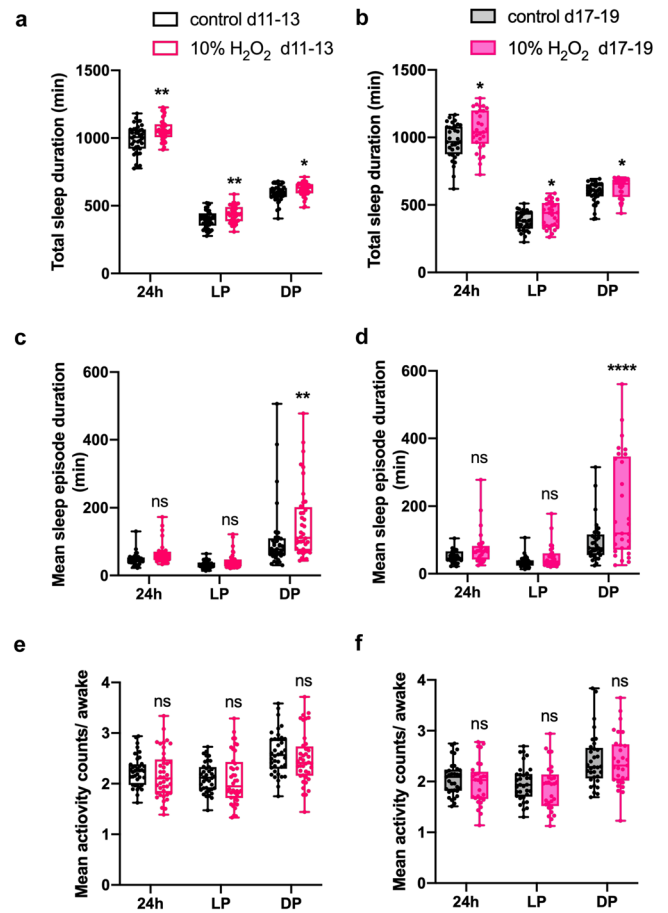


Fig. 7 | A single short-term H₂O₂ treatment increases nighttime sleep. Seven-day-old *w¹¹¹⁸* flies were treated with 10% H₂O₂ or water for 4 h starting at ZT20 in LD and then placed in the activity monitor. The sleep and activity of flies from age day 11 to 13 (d11-13) (control, *n* = 38; H₂O₂, *n* = 40 flies) and day 17 to 19 (d17-19) (control, *n* = 33; H₂O₂, *n* = 29 flies) were analyzed. **a, b** Total sleep duration over 24 h (24h), during daytime (light period, LP) and the night (dark period, DP) in water-only control and H₂O₂-treated flies from day 11 to 13 (**a**) and day 17 to 19 (**b**). H₂O₂-treated flies show an increase in total sleep in both age groups. **p* < 0.05 and ***p* < 0.01 (two-way ANOVA with Šidák's multiple comparisons test). **c, d** Mean sleep episode duration from day 11 to 13 (**c**) and day 17 to 19 (**d**). H₂O₂-treated flies show an increase in nighttime sleep episode duration in both age groups. ***p* < 0.01 and *****p* < 0.0001 (two-way ANOVA with Šidák's multiple comparisons test). **e, f** Mean activity counts during the wake period from day 11 to 13 (**e**) and day 17 to 19 (**f**). No significant difference was observed between the control and treated groups (two-way ANOVA with Šidák's multiple comparisons test). Source data are provided as a Source Data file.

clear the debris. The absorbance of the supernatant was measured at 625 nm on a spectrophotometer. The measured value was divided by the number of flies homogenized in one tube.

ROS detection

MitoSOX Red (Invitrogen, M36008), a cell-permeable mitochondrial superoxide indicator, was used to measure endogenous ROS levels. Male flies were decapitated, and brains were dissected in Hanks' Balanced Salt Solution (HBSS), followed by incubation in 5 μM MitoSOX for 15 min at 37 °C and three washes with warm HBSS. The brains were mounted in HBSS and imaged immediately with a Leica TCS SP5 confocal microscope or a Nikon Ax confocal microscope.

trans-Tango

The *trans*-Tango assay was performed as described previously⁴³. Briefly, male flies were aged for 10 days at 18 °C to maximize *trans*-

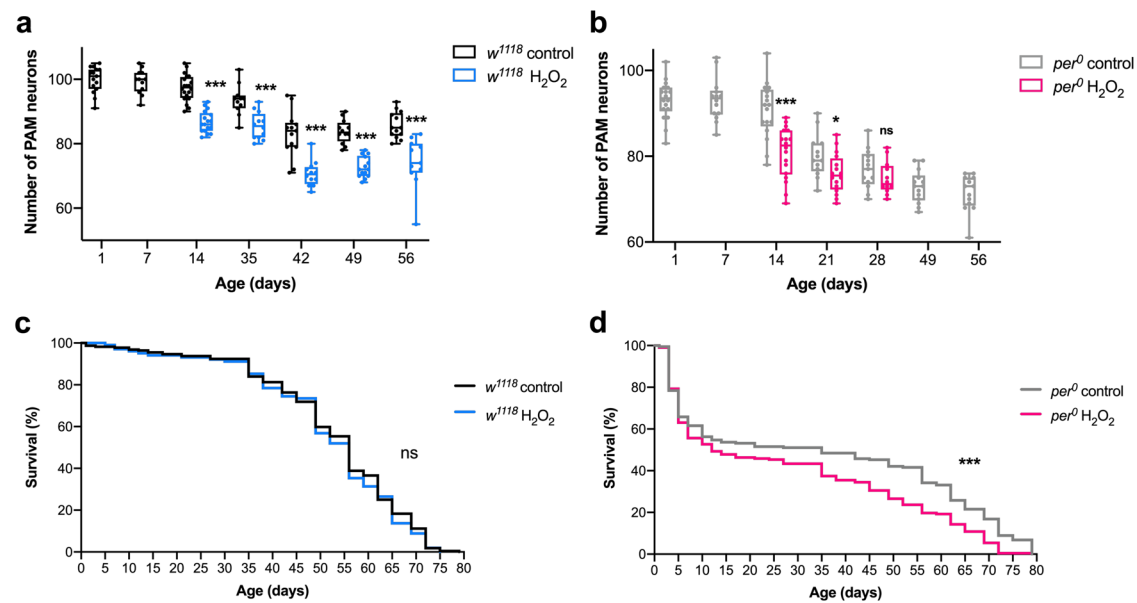


Fig. 8 | A single short-term H₂O₂ treatment causes premature death in *per*⁰ flies.

PAM neuron counts and survival of *w*¹¹¹⁸ and *per*⁰ flies following a 4-h exposure to 10% H₂O₂ at ZT20 when flies were 7 days old. **a, b** PAM neuron counts across aging in *w*¹¹¹⁸ (**a**) and *per*⁰ (**b**). PAM neuron loss was observed as early as day 14 in both genotypes compared to control groups treated with water only. Neurodegeneration progresses with age but is not accelerated in H₂O₂-treated flies. **p* = 0.02 and ****p* < 0.001 (two-tailed *t*-test). *n* = 12–20 hemispheres (see Source Data for individual sample numbers). Since H₂O₂-*per*⁰ flies exhibited a high mortality rate after 28 days, PAM neurons of this group were not examined thereafter. **c, d** % of

surviving flies in *w*¹¹¹⁸ (**c**) and *per*⁰ (**d**). H₂O₂ treatment did not affect the survival of *w*¹¹¹⁸ flies, whereas H₂O₂-treated *per*⁰ flies had significantly reduced lifespans compared to the water-treated control group. ****p* = 0.0002 (Log-rank test). In (**c**), *n* = 3 independent experiments for both control and H₂O₂ treatment, with a total of *n* = 324 *w*¹¹¹⁸ flies for control and *n* = 262 for H₂O₂ treatment. In (**d**), *n* = 3 independent experiments for both the control and the H₂O₂-treated groups, with a total of *n* = 190 *per*⁰ flies for the control and *n* = 203 for the H₂O₂-treated group. Source data are provided as a Source Data file.

Tango expression with the optimal signal-to-noise ratio. The immunohistochemistry protocol described above was used to visualize the neurons and their projections.

In vivo calcium imaging

The calcium sensor GCaMP7s⁴⁸ was expressed with MB299B split-GAL4, and the 3-day-old flies were entrained to LD cycles for 4 days. On the first day in DD following the LD entrainment, flies were placed under the fluorescence microscope in the perfusion chamber after the brief operation to remove a small part of the cuticle of the head capsule. Each experiment consisted of a session of 6-h to 8-h live imaging at 30-min intervals, starting at four different circadian times (CT4, CT10, CT16, and CT22). During each session, 4 flies were recorded, and on average, 13 (ranging from 5 to 19) GFP-positive neurons were imaged per fly. Images were acquired using the Leica DM550 fluorescent microscope. The exposed brains were constantly perfused with oxygenated saline to prevent desiccation or deterioration of the tissue during imaging. Throughout the experiment, the flies retained the ability to move their abdomen and legs. The death of a fly was determined by the absence of movement. Additionally, a sudden drop in fluorescence intensity and a rapid increase in background autofluorescence were considered indicators of tissue deterioration. Data from the flies that died or displayed signs of deterioration during the experiment were excluded from the analysis. The fluorescence intensity of individual cells was measured using the freehand selection tool of Fiji/ImageJ. The corrected total cell fluorescence (CTCF) value was obtained by subtracting the measured fluorescence value outside of MB299B neurons from the measured fluorescence value inside MB299B neurons. The following formula was applied to calculate CTCF: CTCF = integrated density - (area of the region of interest × mean fluorescence of background). The mean of the CTCF of individual cells per timepoint was calculated, and the normalized CTCF time

series was obtained by dividing the mean CTCF of each timepoint by the lowest mean CTCF over 24 h.

Sleep assay and data analysis

The fly sleep assay was performed as described previously with minor modifications²⁷. Seven-day-old male flies were deprived of food and water for 5 h and treated with 10% H₂O₂ for 4 h starting at ZT20. The control group was treated with water only. After the treatment, flies were placed in individual glass tubes containing 5% agarose with 2% sucrose in the *Drosophila* Activity Monitoring (DAM) System 3 (Trikinetics) and entrained in 12 h:12 h-LD cycles at 25 °C for 3 days. Locomotor activity data were recorded during the subsequent 12 days in LD. We extracted sleep quantity from the activity data collected in 1-min bins (defined as bouts of inactivity lasting for 5 min or longer)⁷³. Sleep analysis was performed in MATLAB (MathWorks, version R2017a) using SCAMP v2 (Sleep and Circadian Analysis MATLAB Program) according to the instruction manual (Vecsey laboratory)⁷⁴. *MB299B>Shi^{TS}* and *UAS-Shi^{TS}* flies were raised at 19 °C in 12 h:12 h-LD cycles until 7 days old and placed in the activity monitor at 19 °C, 12 h:12 h-LD cycles. When they were 11 days old, the temperature was shifted to 30 °C until the end of the experiment. Locomotor activity and sleep data between day 11 and 13 were analyzed as described above.

Startle-induced negative geotaxis assay

The startle-induced negative geotaxis assay was performed as previously described⁷⁵ with minor modifications²¹. Twenty male flies were anesthetized with CO₂ and placed in a 100-ml graduated glass cylinder. The cylinder was divided into five equal zones and graded from 1 to 5 from the bottom to the top. The bottom of the cylinder was marked as zone 0. After 1 h of recovery from the CO₂ exposure, the climbing assay was performed at ZT2. Flies were gently tapped to the bottom of the

column to startle them, from which they recovered quickly and started climbing the cylinder wall. The whole experiment was video-recorded for subsequent analyses. The number of flies that climbed up to each zone within the 20 s after startling was manually calculated, from which climbing index (CI) was calculated using the following formula: $CI = (0 \times n_0 + 1 \times n_1 + 2 \times n_2 + 3 \times n_3 + 4 \times n_4 + 5 \times n_5) / n_{total}$, where n_{total} is the number of total flies used in the experiment and n_x is the number of flies that reached the zone X. Three trials for each experimental group were performed at 30-s intervals, from which the median values were chosen as final data of an experiment. Three to four independent experiments were performed per group per age.

Lifespan assay

Lifespans of flies were assayed as previously described with minor modifications⁷⁶. Briefly, 1-day-old male flies were placed in the vials containing cornmeal agar food, 10 flies per vial, and maintained under 12 h:12 h-LD cycles at 25 °C. At 7 days old, treatment groups were exposed to 10% H₂O₂ for 4 h starting at ZT20, as described above. Control groups were treated with water only. Following the treatment, flies were returned to the vials with food. Flies were transferred to new vials twice a week, and the number of dead flies was recorded daily throughout the experiment.

Confocal microscopy and image analysis

Fly brains were imaged using a Leica TCS SP5 confocal microscope and a Nikon Ax confocal microscope. All images were analyzed using Fiji/ImageJ software (NIH). To count DA neurons, neurons positive for TH immunostaining or neurons labeled with fluorescent protein were counted manually using the cell-counter plugin of ImageJ through individual Z-stacks of the confocal images. To quantify the fluorescence intensity of the MitoSOX Red in the region of PAM neurons expressing GFP, the measurement feature of ImageJ was used after adjusting a proper threshold. To calculate the resulting fluorescence intensity of the MitoSOX Red in the region of PAM neurons, the CTCF value was obtained by subtracting the measured fluorescence value outside of the PAM region from the measured fluorescence value inside PAM neurons.

Statistical analysis. GraphPad Prism (v.8.1) and R were used for statistical analysis and data plotting. All data were assessed using the D'Agostino-Pearson normality test. No statistical method was used to predetermine the sample size. Sample sizes were chosen without calculation but based on the literature describing similar experiments. Investigators were not blinded to genotypes and conditions in most experiments because only one experimenter has conducted the entire course of these experiments. However, all data were analyzed using unbiased statistical methods. Experiments performed by multiple investigators (Figs. 2a–d, 3d, e, 4c, 8c, d, and Supplementary Figs. S2a, b, and S7a–c) were analyzed blindly to the genotype and conditions. Normally distributed data were compared using parametric tests, and non-normally distributed data were analyzed using nonparametric tests. To compare the two groups, the two-tailed Student's *t*-test was used for normally distributed data, and for non-normally distributed data, the nonparametric Mann–Whitney test was used. To compare three or more groups of normally distributed data, one-way analysis of variance (ANOVA) with post hoc Tukey's multiple comparison test and two-way ANOVA with Šidák's multiple comparisons test were used. The Kruskal–Wallis one-way ANOVA with Dunn's multiple comparison test was used to compare non-normally distributed data. The statistical significance threshold for all experiments was set at $p < 0.05$. In all figures, stars represent statistical significance: * $p < 0.05$, ** $p < 0.01$, *** $p < 0.001$, and **** $p < 0.0001$. ns indicates not significant. Micrographs are representatives of two or more independent experiments. The box boundaries of all box plots are the 25th and 75th percentiles,

the horizontal line across the box is the median, and the whiskers indicate the minimum and maximum values. All data points are displayed.

Reporting summary

Further information on research design is available in the Nature Portfolio Reporting Summary linked to this article.

Data availability

All data are available in the main text or the supplementary materials. Source data are provided with this paper.

References

1. Fifel, K. & Videnovic, A. Circadian and sleep dysfunctions in neurodegenerative disorders—an update. *Front. Neurosci.* **14**, 627330 (2021).
2. Shulman, J. M., De Jager, P. L. & Feany, M. B. Parkinson's disease: genetics and pathogenesis. *Annu. Rev. Pathol.* **6**, 193–222 (2011).
3. Leng, Y. et al. Association of circadian abnormalities in older adults with an increased risk of developing Parkinson disease. *JAMA Neurol.* **77**, 1270–1278 (2020).
4. Liu, W.-W. et al. BMAL1 regulation of microglia-mediated neuroinflammation in MPTP-induced Parkinson's disease mouse model. *FASEB J.* **34**, 6570–6581 (2020).
5. French, I. T. & Muthusamy, K. A. A review of sleep and its disorders in patients with Parkinson's disease in relation to various brain structures. *Front. Aging Neurosci.* **8**, 114 (2016).
6. Lu, B. & Vogel, H. *Drosophila* models of neurodegenerative diseases. *Annu. Rev. Pathol. Mech. Dis.* **4**, 315–342 (2009).
7. Whitworth, A. J. *Drosophila* models of Parkinson's disease. *Adv. Genet.* **73**, 1–50 (2011).
8. Nagoshi, E. *Drosophila* models of sporadic Parkinson's disease. *Int. J. Mol. Sci.* **19**, 3343 (2018).
9. Mao, Z. & Davis, R. L. Eight different types of dopaminergic neurons innervate the *Drosophila* mushroom body neuropil: anatomical and physiological heterogeneity. *Front. Neural Circuits* **3**, 5 (2009).
10. Aryal, B. & Lee, Y. Disease model organism for Parkinson disease: *Drosophila melanogaster*. *BMB Rep.* **52**, 250–258 (2019).
11. Navarro, J. A. et al. Analysis of dopaminergic neuronal dysfunction in genetic and toxin-induced models of Parkinson's disease in *Drosophila*. *J. Neurochem.* **131**, 369–382 (2014).
12. Miozzo, F. et al. Maintenance of mitochondrial integrity in midbrain dopaminergic neurons governed by a conserved developmental transcription factor. *Nat. Commun.* **13**, 1426 (2022).
13. Tas, D. et al. Parallel roles of transcription factors dFOXO and FER2 in the development and maintenance of dopaminergic neurons. *PLoS Genet.* **14**, e1007271 (2018).
14. Riemensperger, T. et al. A single dopamine pathway underlies progressive locomotor deficits in a *Drosophila* model of Parkinson disease. *Cell Rep.* **5**, 952–960 (2013).
15. Pütz, S. M. et al. Loss of p21-activated kinase Mbt/PAK4 causes Parkinson-like symptoms in *Drosophila*. *Dis. Models Mech.* **14**, dmm047811 (2021).
16. Liu, C. et al. A subset of dopamine neurons signals reward for odour memory in *Drosophila*. *Nature* **488**, 512–516 (2012).
17. Yamagata, N. et al. Distinct dopamine neurons mediate reward signals for short- and long-term memories. *Proc. Natl Acad. Sci. USA* **112**, 578–583 (2015).
18. Landayan, D., Feldman, D. S. & Wolf, F. W. Satiation state-dependent dopaminergic control of foraging in *Drosophila*. *Sci. Rep.* **8**, 5777 (2018).
19. Jacob, P. F. & Waddell, S. Spaced training forms complementary long-term memories of opposite valence in *Drosophila*. *Neuron* **106**, 977–991.e4 (2020).

20. Driscoll, M. et al. Compartment specific regulation of sleep by mushroom body requires GABA and dopaminergic signaling. *Sci. Rep.* **11**, 20067 (2021).
21. Bou Dib, P. et al. A conserved role for p48 homologs in protecting dopaminergic neurons from oxidative stress. *PLoS Genet.* **10**, e1004718 (2014).
22. Hardin, P. E. & Panda, S. Circadian timekeeping and output mechanisms in animals. *Curr. Opin. Neurobiol.* **23**, 724–731 (2013).
23. Hall, J. C. Genetics and molecular biology of rhythms in *Drosophila* and other insects. *Adv. Genet.* **48**, 1–280 (2003).
24. Shafer, O. T. et al. Connectomic analysis of the *Drosophila* lateral neuron clock cells reveals the synaptic basis of functional pacemaker classes. *eLife* **11**, e79139 (2022).
25. Reinhard, N. et al. The neuronal circuit of the dorsal circadian clock neurons in *Drosophila melanogaster*. *Front. Physiol.* **13**, 886432 (2022).
26. Kozlov, A. & Nagoshi, E. Decoding *Drosophila* circadian pacemaker circuit. *Curr. Opin. Insect Sci.* **36**, 33–38 (2019).
27. Machado Almeida, P., Lago Solis, B., Stickley, L., Feidler, A. & Nagoshi, E. *Neurofibromin 1* in mushroom body neurons mediates circadian wake drive through activating cAMP–PKA signaling. *Nat. Commun.* **12**, 5758 (2021).
28. Potdar, S. & Sheeba, V. Wakefulness is promoted during day time by PDFR signalling to dopaminergic neurons in *Drosophila melanogaster*. *eNeuro* **5**, ENEURO.0129–18.2018 (2018).
29. Liang, X. et al. Morning and evening circadian pacemakers independently drive premotor centers via a specific dopamine relay. *Neuron* **102**, 843–857.e4 (2019).
30. Rijo-Ferreira, F. & Takahashi, J. S. Genomics of circadian rhythms in health and disease. *Genome Med.* **11**, 82 (2019).
31. Krishnan, N., Davis, A. J. & Giebultowicz, J. M. Circadian regulation of response to oxidative stress in *Drosophila melanogaster*. *Biochem. Biophys. Res. Commun.* **374**, 299–303 (2008).
32. Boomgarden, A. C. et al. Chronic circadian misalignment results in reduced longevity and large-scale changes in gene expression in *Drosophila*. *BMC Genomics* **20**, 14 (2019).
33. Vaccaro, A., Issa, A.-R., Seugnet, L., Birman, S. & Klarsfeld, A. *Drosophila* clock is required in brain pacemaker neurons to prevent premature locomotor aging independently of its circadian function. *PLoS Genet.* **13**, e1006507 (2017).
34. Krishnan, N., Kretzschmar, D., Rakshit, K., Chow, E. & Giebultowicz, J. M. The circadian clock gene period extends healthspan in aging *Drosophila melanogaster*. *Aging* **1**, 937–948 (2009).
35. Edgecomb, R. S., Harth, C. E. & Schneiderman, A. M. Regulation of feeding behavior in adult *Drosophila melanogaster* varies with feeding regime and nutritional state. *J. Exp. Biol.* **197**, 215–235 (1994).
36. Xu, K., Zheng, X. & Sehgal, A. Regulation of feeding and metabolism by neuronal and peripheral clocks in *Drosophila*. *Cell Metab.* **8**, 289–300 (2008).
37. Pei, J.-F. et al. Diurnal oscillations of endogenous H₂O₂ sustained by p66Shc regulate circadian clocks. *Nat. Cell Biol.* **21**, 1553–1564 (2019).
38. Gummadova, J. O., Coutts, G. A. & Glossop, N. R. J. Analysis of the *Drosophila* clock promoter reveals heterogeneity in expression between subgroups of central oscillator cells and identifies a novel enhancer region. *J. Biol. Rhythms* **24**, 353–367 (2009).
39. Park, J. H. et al. Differential regulation of circadian pacemaker output by separate clock genes in *Drosophila*. *Proc. Natl Acad. Sci. USA* **97**, 3608–3613 (2000).
40. Kaneko, M., Helfrich-Förster, C. & Hall, J. C. Spatial and temporal expression of the period and timeless genes in the developing nervous system of *Drosophila*: newly identified pacemaker candidates and novel features of clock gene product cycling. *J. Neurosci.* **17**, 6745–6760 (1997).
41. Bahn, J. H., Lee, G. & Park, J. H. Comparative analysis of Pdf-mediated circadian behaviors between *Drosophila melanogaster* and *D. virilis*. *Genetics* **181**, 965–975 (2009).
42. Schubert, F. K., Hagedorn, N., Yoshii, T., Helfrich-Förster, C. & Rieger, D. Neuroanatomical details of the lateral neurons of *Drosophila melanogaster* support their functional role in the circadian system. *J. Comp. Neurol.* **526**, 1209–1231 (2018).
43. Talay, M. et al. Transsynaptic mapping of second-order taste neurons in flies by trans-Tango. *Neuron* **96**, 783–795.e4 (2017).
44. Aso, Y. et al. The neuronal architecture of the mushroom body provides a logic for associative learning. *eLife* **3**, e04577 (2014).
45. Dionne, H., Hibbard, K. L., Cavallaro, A., Kao, J.-C. & Rubin, G. M. Genetic reagents for making split-GAL4 lines in *Drosophila*. *Genetics* **209**, 31–35 (2018).
46. Scheffer, L. K. et al. A connectome and analysis of the adult *Drosophila* central brain. *eLife* **9**, e57443 (2020).
47. Plaza, S.M. et al. neuPrint: An open access tool for EM connectomics. *Front. Neuroinform.* **16**, 896292 (2022).
48. Dana, H. et al. High-performance calcium sensors for imaging activity in neuronal populations and microcompartments. *Nat. Methods* **16**, 649–657 (2019).
49. Baines, R. A., Uhler, J. P., Thompson, A., Sweeney, S. T. & Bate, M. Altered electrical properties in *Drosophila* neurons developing without synaptic transmission. *J. Neurosci.* **21**, 1523–1531 (2001).
50. Sitaraman, D., Aso, Y., Rubin, G. M. & Nitabach, M. N. Control of sleep by dopaminergic inputs to the *Drosophila* mushroom body. *Front. Neural Circuits* **9**, 73 (2015).
51. Mabuchi, I. et al. Mushroom body signaling is required for locomotor activity rhythms in *Drosophila*. *Neurosci. Res.* **111**, 25–33 (2016).
52. Kilman, V. L., Zhang, L., Meissner, R.-A., Burg, E. & Allada, R. Perturbing dynamin reveals potent effects on the *Drosophila* circadian clock. *PLoS ONE* **4**, e5235 (2009).
53. Carvey, P. M., Punati, A. & Newman, M. B. Progressive dopamine neuron loss in Parkinson’s disease: the multiple hit hypothesis. *Cell Transpl.* **15**, 239–250 (2006).
54. Gonzalez, M. C., Dalen, I., Maple-Grødem, J., Tysnes, O.-B. & Alves, G. Parkinson’s disease clinical milestones and mortality. *NPJ Parkinsons Dis.* **8**, 1–5 (2022).
55. Ali, F. & Kwan, A. C. Interpreting in vivo calcium signals from neuronal cell bodies, axons, and dendrites: a review. *Neurophotonics* **7**, 011402 (2020).
56. Johard, H. A. D. et al. Peptidergic clock neurons in *Drosophila*: ion transport peptide and short neuropeptide F in subsets of dorsal and ventral lateral neurons. *J. Comp. Neurol.* **516**, 59–73 (2009).
57. Vecsey, C. G., Pírez, N. & Griffith, L. C. The *Drosophila* neuropeptides PDF and sNPF have opposing electrophysiological and molecular effects on central neurons. *J. Neurophysiol.* **111**, 1033–1045 (2014).
58. Montague, S. A. & Baker, B. S. Memory elicited by courtship conditioning requires mushroom body neuronal subsets similar to those utilized in appetitive memory. *PLoS ONE* **11**, e0164516 (2016).
59. Liang, X., Holy, T. E. & Taghert, P. H. A series of suppressive signals within the *Drosophila* circadian neural circuit generates sequential daily outputs. *Neuron* **94**, 1173–1189.e4 (2017).
60. Ulgherait, M. et al. Circadian regulation of mitochondrial uncoupling and lifespan. *Nat. Commun.* **11**, 1927 (2020).
61. Nall, A. H. et al. Caffeine promotes wakefulness via dopamine signaling in *Drosophila*. *Sci. Rep.* **6**, 20938 (2016).
62. Ichinose, T. et al. Reward signal in a recurrent circuit drives appetitive long-term memory formation. *eLife* **4**, e10719 (2015).
63. Lyons, L. C. & Roman, G. Circadian modulation of short-term memory in *Drosophila*. *Learn Mem.* **16**, 19–27 (2009).
64. Chouhan, N. S., Wolf, R., Helfrich-Förster, C. & Heisenberg, M. Flies remember the time of day. *Curr. Biol.* **25**, 1619–1624 (2015).

65. Flyer-Adams, J. G. et al. Regulation of olfactory associative memory by the circadian clock output signal pigment-dispersing factor (PDF). *J. Neurosci.* **40**, 9066–9077 (2020).
 66. Scorza, F. A. et al. Sudden unexpected death in Parkinson's disease (SUDPAR): a review of publications since the decade of the brain. *Clinics* **72**, 649–651 (2017).
 67. Claridge-Chang, A. et al. Writing memories with light-addressable reinforcement circuitry. *Cell* **139**, 405–415 (2009).
 68. Grima, B., Chélot, E., Xia, R. & Rouyer, F. Morning and evening peaks of activity rely on different clock neurons of the *Drosophila* brain. *Nature* **431**, 869–873 (2004).
 69. Vosshall, L. B., Price, J. L., Sehgal, A., Saez, L. & Young, M. W. Block in nuclear localization of period protein by a second clock mutation, timeless. *Science* **263**, 1606–1609 (1994).
 70. Renn, S. C., Park, J. H., Rosbash, M., Hall, J. C. & Taghert, P. H. A pdf neuropeptide gene mutation and ablation of PDF neurons each cause severe abnormalities of behavioral circadian rhythms in *Drosophila*. *Cell* **99**, 791–802 (1999).
 71. Blanchardon, E. et al. Defining the role of *Drosophila* lateral neurons in the control of circadian rhythms in motor activity and eclosion by targeted genetic ablation and PERIOD protein overexpression. *Eur. J. Neurosci.* **13**, 871–888 (2001).
 72. Kitamoto, T. Conditional modification of behavior in *Drosophila* by targeted expression of a temperature-sensitive shibire allele in defined neurons. *J. Neurobiol.* **47**, 81–92 (2001).
 73. Shaw, P. J., Cirelli, C., Greenspan, R. J. & Tononi, G. Correlates of sleep and waking in *Drosophila melanogaster*. *Science* **287**, 1834–1837 (2000).
 74. Donelson, N. et al. High-resolution positional tracking for long-term analysis of *Drosophila* sleep and locomotion using the “Tracker” program. *PLoS ONE* **7**, e37250 (2012).
 75. Friggi-Grelin, F. et al. Targeted gene expression in *Drosophila* dopaminergic cells using regulatory sequences from tyrosine hydroxylase. *J. Neurobiol.* **54**, 618–627 (2003).
 76. Piper, M. D. W. & Partridge, L. Protocols to study aging in *Drosophila*. *Methods Mol. Biol.* **1478**, 291–302 (2016).
- Foundation to E.N., Ernst and Lucie Schmidheiny to EN Société Académique de Genève to E.N.

Author contributions

Conceptualization: M.M.D. and E.N. Investigation: M.M.D., L.C.D., and E.P. Visualization: M.M.D., L.C.D., E.P., and E.N. Writing: M.M.D., L.C.D., and E.N.

Competing interests

The authors declare no competing interests.

Additional information

Supplementary information The online version contains supplementary material available at <https://doi.org/10.1038/s41467-023-41540-y>.

Correspondence and requests for materials should be addressed to Emi Nagoshi.

Peer review information *Nature Communications* thanks Sean Sweeney and the other anonymous reviewer(s) for their contribution to the peer review of this work. A peer review file is available.

Reprints and permissions information is available at <http://www.nature.com/reprints>

Publisher's note Springer Nature remains neutral with regard to jurisdictional claims in published maps and institutional affiliations.

Open Access This article is licensed under a Creative Commons Attribution 4.0 International License, which permits use, sharing, adaptation, distribution and reproduction in any medium or format, as long as you give appropriate credit to the original author(s) and the source, provide a link to the Creative Commons licence, and indicate if changes were made. The images or other third party material in this article are included in the article's Creative Commons licence, unless indicated otherwise in a credit line to the material. If material is not included in the article's Creative Commons licence and your intended use is not permitted by statutory regulation or exceeds the permitted use, you will need to obtain permission directly from the copyright holder. To view a copy of this licence, visit <http://creativecommons.org/licenses/by/4.0/>.

© The Author(s) 2023

Acknowledgements

We thank Dong-gen Luo for helpful technical advice and the Bloomington *Drosophila* Stock Center and Kyoto Stock Center for fly strains. We also thank Ralf Stanewsky for a fly strain and Serge Birman for comments on the manuscript. The following funding sources supported this research: Swiss National Science Foundation grants to E.N. (31003A_169548 and 310030_189169), Georges and Antoine Claraz